NASA TECHNICAL NOTE

NASA TN D-5296

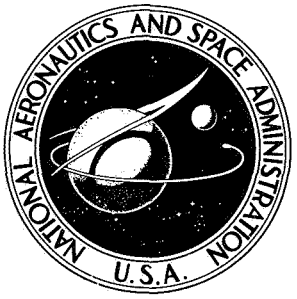

NASA TN D-5296

INFLATION AND PERFORMANCE OF THREE PARACHUTE CONFIGURATIONS FROM SUPERSONIC FLIGHT TESTS IN A LOW-DENSITY ENVIRONMENT

by Charles H. Whitlock and Richard J. Bendura

Langley Research Center
Langley Station, Hampton, Va.

NATIONAL AERONAUTICS AND SPACE ADMINISTRATION • WASHINGTON, D. C. • JULY 1969

NASA TN D-5296

INFLATION AND PERFORMANCE OF THREE PARACHUTE CONFIGURATIONS FROM SUPERSONIC FLIGHT TESTS IN A LOW-DENSITY ENVIRONMENT

By Charles H. Whitlock and Richard J. Bendura

Langley Research Center
Langley Station, Hampton, Va.

NATIONAL AERONAUTICS AND SPACE ADMINISTRATION

For sale by the Clearinghouse for Federal Scientific and Technical Information
Springfield, Virginia 22151 – CFSTI price $3.00

INFLATION AND PERFORMANCE OF THREE PARACHUTE CONFIGURATIONS FROM SUPERSONIC FLIGHT TESTS IN A LOW-DENSITY ENVIRONMENT

By Charles H. Whitlock and Richard J. Bendura
Langley Research Center

SUMMARY

Ten flight tests of modified-ringsail, disk-gap-band, and cross parachute configurations with deployment initiated at Mach numbers and dynamic pressures corresponding to conditions expected during entry into a Martian atmosphere have been completed. Comparison of flight results indicates that theoretical snatch force values were never exceeded when the deployment techniques of these tests were used. Opening loads showed no definite trend with Mach number. Values for filling times compared favorably with generally accepted empirical curves based on 15-percent geometric porosity. Canopy stability was good when Mach numbers were below 1.4 for the modified-ringsail and disk-gap-band configurations. At higher Mach numbers, one test of the disk-gap-band configuration showed canopy fluctuations. The cross-parachute canopies did not achieve a stable configuration during the data period. Comparison of the drag coefficients indicates that the cross parachute produced the highest values, and the modified-ringsail values were slightly higher than those of the disk-gap-band configuration.

INTRODUCTION

The Langley Research Center has conducted two programs for a total of 10 tests the objective of which was to obtain free-flight parachute performance data on inflation, drag, and stability characteristics at Mach numbers and dynamic pressures corresponding to those which might be encountered during entry into the atmosphere of Mars. (See ref. 1.) These programs were called the Planetary Entry Parachute Program (PEPP) and the Supersonic Planetary Entry Decelerator Program, Part I, (SPED I). The PEPP experiments used both balloon-launched and rocket-launched techniques to test disk-gap-band, modified-ringsail, and cross parachute configurations in the low-density environment at earth altitudes greater than 100 000 ft (30.48 km). (See ref. 2.) Deployment Mach numbers ranged from 1.15 to 1.64 at dynamic pressures from 5.82 to 11.0 lb/ft^2 (278 to 526 N/m^2). Results from the rocket-launched portion of PEPP are described in references 3 to 6, and the results of the balloon-launched experiments are described in

references 7 to 10. The SPED I program was an extension of the rocket-launched portion of PEPP. Disk-gap-band parachutes and a ram-air-inflated ballute decelerator were deployed at Mach numbers from 1.91 to 3.15 at dynamic pressures from 9.7 to 38.5 lb/ft^2 (460 to 1850 N/m^2). Results from the SPED I tests are described in references 11 to 13.

The purpose of this paper is to summarize and analyze the inflation and drag data of the disk-gap-band, modified-ringsail, and cross parachutes obtained during the PEPP and SPED I flight tests. Inflation loads, filling times, filling distances, canopy fluctuations, and drag characteristics are compared for each type of parachute. No analysis of the ballute data is included in this report.

SYMBOLS

a_X axial acceleration, g units

a_Y transverse acceleration to vehicle center line, g units

a_N normal acceleration to vehicle center line, g units

C_D drag coefficient, $\frac{\text{Drag}}{q_\infty S}$

$C_{D,o}$ drag coefficient based on nominal parachute area, S_o

C_DS drag area, feet^2 (meters^2)

$(C_{D,o})_{eff}$ effective drag coefficient based on vertical velocity during descent

D_o nominal diameter $(4S_o/\pi)^{1/2}$, feet (meters)

F_p maximum force, pounds (newtons)

g acceleration due to gravity, feet per second^2 (meters per second^2)

L_S length of suspension lines, feet (meters)

M Mach number

m mass, slugs (kilograms)

m_c mass of canopy, slugs (kilograms)

m_s	combined mass of parachute and payload, slugs (kilograms)
N	number of gores
P_M	measured snatch force, pounds (newtons)
P_T	theoretical snatch force, pounds (newtons)
P'	breaking strength of suspension lines, pounds (newtons)
q_∞	free-stream dynamic pressure, pounds per foot^2 (newtons per meter^2)
q_w	dynamic pressure in wake, pounds per foot^2 (newtons per meter^2)
S	area, feet^2 (meters^2)
S_o	surface area of parachute (includes gaps, slots, and vents for disk-gap-band and modified-ringsail configurations), feet^2 (meters^2)
S_p	projected area of canopy including gaps, slots, and vents, feet^2 (meters^2)
T	tensiometer range, pounds (newtons)
t	time, seconds
t_f	filling time, seconds
V	free-stream velocity, feet per second (meters per second)
V_R	relative velocity between deployment bag and towing spacecraft, feet per second (meters per second)
W_d	descent weight (parachute plus payload), pounds (kilograms)
W_m	canopy cloth weight per unit area, ounces per yard^2 (grams per meter^2)
W_p	weight of parachute including upper riser, pounds (kilograms)
X	distance traveled during canopy inflation, feet (meters)

Z number of suspension lines

γ flight-path angle, positive up, degrees

ΔL elongation in suspension lines at breaking load, feet (meters)

Δp differential pressure, inches H_2O (centimeters H_2O)

Δt time increment from mortar fire to line stretch, seconds

ΔV_V change in velocity of the towing spacecraft between the times of mortar fire and line stretch, feet per second (meters per second)

λ_g geometric porosity, percent

λ_m cloth permeability, feet^3 per minute per foot^2 at 1/2 inch H_2O Δp (meters^3 per minute per meter^2 at 1.27 centimeters H_2O Δp)

$\xi' = \Delta L/L_S$

ρ atmospheric density, slugs per foot^3 (kilograms per meter^3)

Subscripts:

b deployment bag

bs bag-strip conditions

mf deployment (mortar fire) conditions

fi full-inflation conditions

ls line-stretch conditions

Dots over symbols denote time derivatives and bars over symbols denote average values.

PARACHUTE DESCRIPTION

The parachute configurations tested were the disk-gap-band (DGB), modified-ringsail, and cross type. A sketch of each type of configuration is shown in figure 1. For a given nominal diameter, the cross parachute had a larger projected diameter than either of the other two configurations. This condition occurred because the nominal area included the cloth, gaps, and vent for the disk-gap-band and modified-ringsail configurations, but only the cloth area was included for the cross parachute. (The relative sizes are in nearly correct proportion in fig. 1.) Important physical properties of the different parachutes are given in the following table:

Parachute	D_o		L_s		N	λ_g, percent	λ_m (a)		W_m		W_p		W_d	
	ft	m	ft	m					oz/yd^2	g/m^2	lb	kg	lb	kg
Modified ringsail	31.2	9.51	30.0	9.14	24	15	162	49.4	1.9	64	[b]19.8	[b]9.0	221	100
	40.0	12.2	40.0	12.2	36	15	[c]162 [d]1061	[c]49.4 [d]323.4	[c]1.9 [d]1.0	[c]64 [d]34	33.0	15	239	108
	54.5	16.6	64.7	19.7	54	15	162	49.4	1.9	64	72.4	32.8	549	249
	85.3	26.0	78.7	24.0	72	15	1061	323.4	1.0	34	[e]81.1	[e]36.8	[f]597 [f]275	[f]291 [f]125
Disk gap band	30.0	9.14	30.0	9.14	24	15	115	35.1	2.0	68	[g]24.5	[g]11.1	226	103
	40.0	12.2	40.0	12.2	32	12.5	115	35.1	2.0	68	[h]34.0	[h]15.4	280	127
	64.7	19.7	65.9	20.1	72	12.4	[i]63 [j]1061	[i]19 [j]323.4	[i]1.5 [j]1.0	[i]51 [j]34	79.6	36.1	557	253
Cross	30.0	9.14	39.3	12.0	--	---	67	20	2.6	88	31.0	14.1	240	109
	54.4	16.6	67.2	20.5	--	---	38	12	1.25	42	73.6	33.6	566	257

[a]Nominal permeability of the canopy cloth measured in ft^3/min/ft^2 at 1/2 inch H_2O Δp or m^3/min/m^2 at 1.27 cm H_2O Δp.

[b]Includes post-reefing (see ref. 3) lines and rings and upper riser but not the metal end fitting or riser line cutter.

[c]Top ring only.

[d]Remaining rings and sails.

[e]Includes reefing hardware, riser, and bridle.

[f]After ballast release.

[g]Includes torus inflation aid and bottles (not used), post-reefing hardware, risers with metal end fittings, and disconnect link with explosive bolt.

[h]Includes post-reefing lines and rings.

[i]Disk.

[j]Band.

Both the suspension-line length L_s and the number of gores varied in approximate proportion to the nominal diameter D_o. The geometric porosity λ_g was nearly constant for the modified-ringsail configurations but was decreased from 15.0 to 12.5 percent for the DGB tests. The cross parachute had no vent; hence, it had no geometric porosity based on the definition of nominal area for that configuration. The mechanical porosity or permeability λ_m varied significantly depending on which canopy material (expressed in weight/unit area, W_m) was used. The materials of construction varied because "off the shelf" materials were utilized and no attempt was made at optimization or maintaining constant margins of safety between tests. For this reason applying the parachute weight W_p to other size and design conditions may not be valid and detailed analysis using design

procedures for each parachute type such as those described in references 14 to 18 must be considered. The parachute weight W_p includes the canopy, suspension lines, upper riser, and any other hardware attached to the parachute during the test. Tensiometer, bridle, and fitting weights are included with the parachute and payload values in the descent weight W_d.

Both the number and proportion of rings to sails varied between the modified-ringsail parachutes. The 31.2-foot-diameter (9.51-meter) configuration contained three rings, six sails, and a gap (omitted sail) between the second and third sails from the skirt. The 40.0-foot-diameter (12.2-meter) parachute had four rings and six sails, whereas the 54.5-foot-diameter (16.6-meter) canopy had four rings and five sails. The gap was also between the second and third sails in both of these parachutes. The 85.3-foot-diameter (26-meter) canopy contained four rings and eight sails, the gap being located between the fourth and fifth sails. All disk-gap-band canopies were essentially of the same basic configuration, the exceptions being the porosity differences noted in the table. Both cross parachutes had panel width-length ratios of approximately 0.26 and were essentially identical except for size, number of suspension lines, and materials of construction. Detailed descriptions of each test parachute are presented in references 3 to 18.

SPACECRAFT DESCRIPTION

Both rocket-launched and balloon-launched techniques were used for the PEPP experiments. A sketch of the payload configurations for both test techniques is shown in figure 2. The rocket-launched payloads were propelled to test altitude and velocity by two-stage Honest John - Nike rocket systems. (Refs. 3 and 4 give additional information about the rocket system.) The parachute was deployed rearward from the payload during ascent prior to trajectory apogee. Details of the deployment sequence for all the tests are discussed subsequently. In the balloon-launched experiments, the payload was attached inside the aeroshell, and the resulting combination was lifted to high altitude by a balloon system. At float altitude, the aeroshell-payload combination was dropped from beneath the balloon and fell for approximately 4 seconds. A cluster of rocket motors was then ignited and subsequently propelled the aeroshell-payload combination to higher altitudes and velocities. (Refs. 2, 7, and 19 present additional information on the balloon-launch technique.) Shortly after rocket-motor burnout but prior to trajectory apogee, the parachute was deployed rearward from the payload which was still attached inside the aeroshell. During the deployment sequence, connection was severed and the payload was extracted from the aeroshell by the parachute upon inflation. Separate trajectories were then flown by the parachute-payload combination and aeroshell.

The SPED I experiments used the same payload configuration and parachute-deployment sequence as the rocket-launched tests of PEPP. However, a three-stage Honest John - Nike - Nike rocket system was used to propel the payloads to test conditions. (Ref. 11 provides additional information concerning the rocket system.)

Principal instrumentation located onboard the flight spacecraft consisted of accelerometers, tensiometers, and motion-picture cameras. Accelerometer and tensiometer ranges as well as camera orientation and speed are given in the following table for each of the parachute tests:

Parachute	Diameter		Flight technique	a_X, g units	a_Y and a_N, g units	T, lb (N)	Camera orientation	Camera speed, frames/sec
	ft	m						
Modified ringsail	31.2	9.51	Rocket launched	±75	±5	0 to 10 000 (0 to 44 480)	Rearward on payload Forward on payload	64 16
Modified ringsail	40.0	12.2	Rocket launched	±75	±5	0 to 10 000 (0 to 44 480)	Rearward on payload Forward on payload	32 16
Modified ringsail	54.5	16.6	Balloon launched	±50 ±5	±1	0 to 20 000 (0 to 88 960)	Rearward on payload Rearward on payload Sideways on payload Rearward on aeroshell (2)	350 16 16 64
Modified ringsail	85.3	26.0	Balloon launched	±50 ±5	±5	----------	Rearward on payload Sideways on payload Forward on payload Rearward on aeroshell (2)	500 16 16 64
Disk gap band	30.0	9.14	Rocket launched	±75	±5	0 to 10 000 (0 to 44 480)	Rearward on payload Forward on payload	64 16
Disk gap band[a]	40.0	12.2	Rocket launched	±75	±5	[b]0 to 10 000 (0 to 44 480)	Rearward on payload Forward on payload	[c]32 and [d]64 16
Disk gap band	64.7	19.7	Balloon launched	±50 ±5	±1	0 to 20 000 (0 to 88 960)	Rearward on payload Rearward on payload Forward on payload Rearward on aeroshell (2)	350 16 16 64
Cross	30.0	9.14	Rocket launched	±75	±5	0 to 10 000 (0 to 44 480)	Rearward on payload Forward on payload	32 16
Cross	54.4	16.6	Balloon launched	±50 ±5	±1	0 to 20 000 (0 to 88 960)	Rearward on payload Rearward on payload Forward on payload Rearward on aeroshell (2)	350 16 16 64

[a] One test each at $M_{mf} = 1.91$ and $M_{mf} = 2.72$.
[b] No tensiometer data for $M_{mf} = 2.72$ test.
[c] $M_{mf} = 1.91$ test.
[d] $M_{mf} = 2.72$ test.

Accelerometers were located with the payload on each test. When used, the tensiometers were inserted in the bridle-riser system used to attach the parachute to the payload. A tensiometer was not carried during the test of the 85.3-foot (26.0-meter) modified-ringsail parachute. In the case of one of the 40.0-foot (12.2-meter) disk-gap-band tests, the tensiometer connection was accidentally severed during deployment. Loads data were obtained entirely from accelerometer results for these two tests. All rocket-launched tests carried a gyro platform onboard the payload in addition to the instrumentation. Useful attitude data from the gyro platform however were obtained only during the tests of the 31.2-foot (9.51-meter) modified ringsail, the 30.0-foot (9.14-meter) cross, and

the 40.0-foot (12.2-meter) disk-gap-band (M_{mf} = 1.91) parachutes. The accelerometer, tensiometer, and gyro-platform data were telemetered to ground receiving stations for the rocket-launched tests. Overall data inaccuracy is estimated at less than 3 percent of full scale for this type of instrumentation system. For the balloon-launched experiments, accelerometer and tensiometer data were obtained by means of onboard tape recorders which were recovered with the payloads. Accelerometer data inaccuracy was less than 1 percent of full scale because of an in-flight calibration point unique with the balloon-launch technique. All camera data were obtained after payload and aeroshell recovery.

DEPLOYMENT SEQUENCE

The deployment systems for both the rocket-launched and balloon-launched tests were similar in nature. All parachutes were packed in a deployment bag to a density of approximately 40 lb/ft^3 (641 kg/m^3). The deployment bag and packed parachute were inserted into a mortar which was 1 foot (0.30 meter) in diameter and either 1.42 foot (0.43 meter) or 2.6 foot (0.79 meter) in length. (The balloon-launched system utilized the longer mortar of the two sizes.) One end of the deployment bag was attached to the lid of the mortar, and the other (the mouth) was tied closed. The mouth tie was cut immediately after the bag and packed parachute were ejected rearward from the payload by the mortar. Nominal ejection velocity was 120 ft/sec (36.6 m/sec) for the rocket-launched tests and 130 ft/sec (39.6 m/sec) for the balloon-launched flights. As the packed parachute extended rearward, the suspension lines were extracted from the bag until line stretch, at which time a snatch load was recorded, and the canopy began to be extracted from the bag. When the bag had completely stripped from the canopy, a tie in the crown of the parachute was broken and the deployment bag and mortar lid combination separated from the parachute-payload system. After the bag was stripped, the canopy proceeded to inflate. Performance data were recorded during the deployment sequence as well as after full inflation. Figure 3 is a sketch showing the deployment sequence for the two types of tests.

Although the natures of the deployment sequence for the rocket-launched and balloon-launched tests were similar, the environments during the sequence were somewhat dissimilar. The towing body for the rocket-launched series was a lightweight, slender configuration in comparison with the balloon-launched vehicle. The reaction of the deployment mortar caused an acceleration and thus a small increase in velocity at the time of mortar fire. The velocity increase of the payload was approximately 30 ft/sec (9.1 m/sec) for the rocket-launched tests and only about 3 ft/sec (0.9 m/sec) for the balloon-launched spacecraft. The balloon-launched spacecraft also had a higher ratio of drag to weight than the rocket-launched payload and thus caused a significant deceleration of the balloon-launched spacecraft during the deployment sequence in addition to that provided by the

parachute. Longer suspension-line lengths and larger canopy diameters were tested with the balloon-launched technique. As a result, the time intervals between the various events of the deployment sequence were longer than those of the rocket-launched series. The combination of the differences between the payload velocity increases at mortar fire, the decelerations caused by the towing body, and the time intervals between events caused significant differences in the dynamic-pressure history during deployment between the two series of tests. For a typical rocket-launched test, the dynamic pressure at line stretch was approximately 97.3 percent of that at mortar fire whereas line-stretch dynamic pressure was 89 percent of the mortar fire value for the comparable balloon-launched flight as presented in figure 4. Also from figure 4, full-inflation dynamic pressure was 82.5 percent of that at mortar fire for the rocket-launched test as compared with 64 percent for the balloon-launched flight. Similar differences existed for the entire program and are presented in the following table:

Parachute	Diameter		M_{mf}	$q_{\infty,mf}$		$q_{\infty,ls}$		$q_{\infty,fi}$		$\frac{q_{\infty,ls}}{q_{\infty,mf}}$	$\frac{q_{\infty,fi}}{q_{\infty,mf}}$	$\frac{q_{\infty,fi}}{q_{\infty,ls}}$
	ft	m		lb/ft^2	N/m^2	lb/ft^2	N/m^2	lb/ft^2	N/m^2			
Rocket-launched tests												
Modified ringsail	31.2	9.51	1.39	11.0	527	10.8	517	9.4	450	0.975	0.855	0.875
Disk gap band	30.0	9.14	1.56	11.4	546	11.1	531	9.4	450	.973	.825	.846
Cross	30.0	9.14	1.57	9.7	464	9.4	450	8.5	407	.970	.878	.905
Disk gap band	40.0	12.2	1.91	11.6	555	11.3	541	8.0	383	.975	.88	.902
Disk gap band	40.0	12.2	2.72	9.7	464	9.1	436	8.2	393	.94	.845	.900
Balloon-launched tests												
Disk gap band	64.7	19.7	1.59	11.6	555	10.3	493	7.4	354	0.89	0.64	0.72
Modified ringsail	54.5	16.6	1.60	11.6	555	10.3	493	8.1	388	.89	.70	.785
Cross	54.4	16.6	1.65	12.7	608	11.3	541	9.6	460	.89	.755	.85

Values are not presented for the 40.0-foot (12.2-meter) and 85.3-foot (26.0-meter) modified-ringsail tests because the 40.0-foot (12.2-meter) configuration failed to inflate fully (ref. 5) and the 85.3-foot (26.0-meter) parachute was inflated in a reefed condition (ref. 7). In the case of the 40.0-foot (12.2-meter) disk-gap-band parachute deployed at $M_{mf} = 1.91$, the event of full inflation was taken as the first peak of the projected area history (0.80 second after mortar fire) shown in reference 11.

SNATCH FORCES

The snatch force at line stretch is defined as that force imposed upon the suspended payload by the decelerator in order to accelerate the mass of the decelerator from its velocity at line extension to the velocity of the suspended payload. (See ref. 20.) Based on simplified energy balance principles (ref. 20), the snatch force may be theoretically estimated from

$$P_T = \sqrt{\frac{m_c Z P' (V_{R,ls})^2}{L_s \xi'}} \tag{1}$$

The theory assumes that the total mass of the canopy is brought up to the speed of the towing spacecraft as a unit. This assumption does not represent the physical situation for the rocket-launched and balloon-launched tests in which the bag and that portion of the canopy within the bag continued rearward after line stretch to complete the stripping process. Thus the canopy was brought up to the velocity of the payload in segments as it exited the bag. For this reason, the theoretical estimate (eq. (1)) represents a value that would not be exceeded for deployment systems similar to those used on rocket-launched and balloon-launched tests. A comparison of flight-experienced loads with estimates obtained by using equation (1) is shown in figure 5. Theoretical values are based on the estimated weight of the total canopy (excluding suspension lines and riser), average ultimate loads and elongation values from ground test data, and relative velocities at line stretch calculated from flight data as shown in the appendix. Specific values used for the various quantities are given in the following table:

Parachute	Diameter		m_c		Z	P'		L_s		ξ'	P_T		P_M	
	ft	m	slugs	kg		lb	N	ft	m		lb	N	lb	N
Modified ringsail	31.2	9.51	0.522	7.62	24	350	1560	30.0	9.14	0.3	2538	11 290	1700	7 560
Disk gap band	30.0	9.14	.606	8.84	24	600	2670	30.0	9.14	.3	3581	15 930	1300	5 780
Modified ringsail	40.0	12.2	.727	10.6	36	600	2670	40.0	12.2	.3	4232	18 820	1260	5 600
Cross	30.0	9.14	.653	9.53	36	600	2670	39.3	12.0	.3	4151	18 460	1100	4 890
Disk gap band	40.0	12.2	.768	11.2	32	600	2670	40.0	12.2	.3	4312	19 180	1950	8 670
Disk gap band	40.0	12.2	.768	11.2	32	600	2670	40.0	12.2	.3	4031	17 930	2000	8 900
Modified ringsail	85.3	26.0	2.04	29.8	72	350	1560	78.7	24.0	.3	5739	25 530	3250	14 500
Disk gap band	64.7	19.7	1.69	24.7	72	600	2670	65.9	20.1	.3	6442	28 660	1200	5 300
Modified ringsail	54.5	16.6	1.59	23.2	54	600	2670	64.7	19.7	.3	4843	21 540	800	3 600
Cross	54.4	16.6	1.41	20.6	64	600	2670	67.2	20.5	.3	4509	20 060	800	3 600

The estimated weights include such items as post-reefing (see ref. 3) hardware but not the deployment bag and mortar lid combination. Comparison of the actual values with the theoretical values indicates that the calculated estimates do represent a maximum not exceeded by flight results.

OPENING HISTORIES

Histories of the inflation process were obtained by using rearward-looking cameras placed on the payloads. Detailed observation of the film records provided time histories of the projected parachute areas during the inflation process. The inflation profiles from line stretch to full inflation are the subject of this section.

For analysis of the inflation characteristics, it was considered necessary to estimate the times of completion of bag stripping. The purpose was to determine the amount

of parachute inflation which took place while the canopy was still partially constrained by the deployment bag. The precise instant of bag stripping could not be clearly observed from onboard film data on most tests since the bag was obscured by the inflating canopy. Generally, the bag was last seen from onboard cameras during the early part of the stripping process, and then the apex of the canopy was observed without the bag during the early part of inflation. This condition, however, was not true for the cross parachutes. Estimates of the time of bag strip (within 0.05 second) were confirmed from ground tracking telescope camera film for the balloon-launched series of tests. Figures 6, 7, and 8 show portions of these records during the inflation process. Also from these photos, it can be observed that only limited inflation of the modified-ringsail and disk-gap-band parachutes occurred until after bag stripping was complete. The panels of the cross parachute do show significant inflation although portions of the crown are still packed within the deployment bag. Based on these observations, the bag-stripping times for the rocket-launched tests were estimated to occur when the deceleration force was a minimum prior to the rise during inflation for both the modified-ringsail and disk-gap-band parachutes. For the cross parachute, bag stripping was assumed to occur when there was a slight discontinuity in the force history during inflation. Values for the estimated times (from mortar fire) are as follows:

Parachute	Diameter		Bag-stripping time, sec
	ft	m	
Modified ringsail	31.2	9.51	0.47
Modified ringsail	54.5	16.6	.94
Disk gap band	30.0	9.14	.47
Disk gap band	64.7	19.7	1.07
Disk gap band ($M_{mf} = 1.91$)	40.0	12.2	.60
Disk gap band ($M_{mf} = 2.72$)	40.0	12.2	.65
Cross	30.0	9.14	.70
Cross	54.4	16.6	1.17

Histories of the canopy growth during inflation are shown in figures 9, 10, and 11. Presented is the canopy growth parameter (the square root of the ratio of the projected area to the projected area at full inflation) as a function of nondimensionalized time. The time parameter is the time from line stretch divided by the time from line stretch to full inflation. Figure 9 shows the canopy growth history for the modified-ringsail parachute tests. Also shown are the deployment Mach numbers and the points for estimated bag stripping. From this figure it can be observed that the bag-stripping event occurred at significantly different values of the time parameter, but once bag stripping was complete, the growth was somewhat linear to full inflation. The bag-stripping event occurs at different values of the time parameter because the magnitudes of the mortar velocities and suspension-line lengths and canopy radius (which determine the stripping distance)

were different for all tests. If the bag-stripping process hampers inflation, the filling time should be counted as that time from bag stripping to full inflation for systems of the type employed in these tests. Possible reasons for the increased amount of inflation at bag stripping on the rocket-launched tests include (1) the smaller parachute was packed into the same diameter bag as the larger configuration, and (2) whatever dynamic-pressure degradation existed in the wake of the blunt aeroshell was present only for the larger parachute. Figure 10 shows the canopy-growth parameter histories for the disk-gap-band parachute tests. The term "equivalent bag strip" is used for the 30-foot (9.14-meter) configuration because a time period has been subtracted from the total time from line stretch to full inflation owing to the occurrence of an abnormal event. (See ref. 4.) The diameter-ratio history for the balloon-launched 54.5-foot (16.6-meter) cross-parachute test is shown in figure 11. Significant inflation during the bag-stripping process is evident. No results are shown for the 30-foot (9.14-meter) cross-parachute rocket-launched test because the poor quality of the photographs made the determination of a projected-area history impractical.

C_DS $\left(\text{or } \text{Drag}/q_\infty\right)$ as a function of the canopy growth parameter for the modified-ringsail and disk-gap-band parachutes is shown in figures 12 and 13. Results are not presented from the balloon-launch tests because reliable C_DS values could not be obtained while the instrumented payload was sliding within the aeroshell prior to separation during the inflation process. Frictional forces resulted in an unknown amount of drag force being transmitted from the aeroshell to the payload prior to the full inflation. In the case of the Mach 2.72 deployment of the disk-gap-band parachute, elastic effects during the inflation process is a possible cause of the inconsistent data point in figure 13(c). (See ref. 12 for more discussion on elastic effects.)

OPENING LOADS

As discussed previously, the towing body m/C_DS, q_∞ gradient, ejection velocity, suspension-line length, and canopy size were different for each rocket-launched and balloon-launched test. As a result, caution is required when the opening forces experienced during the various flights are compared. One comparison parameter which is relatively independent of deployment system and sequence is $F_p/q_{\infty,fi}S_o$. Use of the dynamic pressure near the time of maximum load to nondimensionalize the force should provide a correlation which is essentially a function of only the parachute and the environment at the time of full inflation. Exclusion of system effects is desirable whenever the test results may be the basis for design of different types of spacecraft. Figure 14 shows the opening force parameter $F_p/q_{\infty,fi}S_o$ as a function of Mach number. No definite trend with Mach number for a particular type of parachute can be established from these data. The two cross-parachute points are reasonably consistent. The four disk-gap-band parachute points indicate a slight increase with Mach number; however, two few data points

exist, particularly in the high Mach number range, to conclude a definite characteristic generally. The two modified-ringsail points show definite disagreement. However, the two canopies were different in size as well as the number and distribution of rings and sails (discussed previously). The parachute which had the highest drag coefficient (to be discussed) also had the highest opening force parameter. Similar effects in terms of the drag characteristics have been observed previously (ref. 21) for ringsail parachute configurations in the 30- to 70-foot-diameter (9.1- to 21.3-meter) range.

During the preliminary stages of design, it is often required to estimate the opening loads when only general trajectory and systems information are known. If the trajectory of the towing spacecraft is known, the time and dynamic pressure of deployment initiation is known. Knowledge of the suspension-line length, canopy length (in the strung-out position) and ejection velocity allows average relative velocities and time intervals from deployment to line stretch and bag stripping to be estimated. Once the time intervals are known, the free-stream dynamic pressures at line stretch and bag stripping can be obtained from the trajectory of the towing spacecraft. Calculation of opening loads based on either the line stretch or bag-stripping dynamic pressure by using a parameter based on these conditions is useful for preliminary estimates and has the advantage of removing most of the system effects (towing spacecraft deceleration, acceleration caused by parachute ejection system, variable time intervals, and so forth) which are present if the dynamic pressure at deployment initiation is used. Detailed calculations using canopy-growth histories and changing deceleration rates during inflation however are required for final analysis.

One correlation which attempts to take into account the effects of deceleration during the inflation process is that suggested by French (ref. 22) and discussed in detail in reference 23. Figure 15 shows the correlation which is the opening-force parameter as a function of a mass parameter. The numerator ρD_o^3 of the mass parameter is proportional to the mass of air enclosed by the canopy, and the denominator is the mass of the combined parachute and payload system. Figure 15(a) is based on bag-stripping conditions and figure 15(b) is in terms of the line-stretch conditions. The present data have been compared with the analytical empirical correlation line taken from experimental data for flat-circular types of parachutes which are generally considered applicable for most parachutes in the higher mass ratio regions. The data from which the empirical correlations were made were very sparse at the low mass ratios which were characteristic of the rocket-launched and balloon-launched tests. The two data points for the disk-gap-band parachute at high mass ratios were obtained from whirltower tests described in reference 4.

Correlation of the opening-force parameter with the mass ratio parameter in terms of line-stretch conditions is of limited value except for the cross parachute. Little drag

was produced by the modified-ringsail and disk-gap-band parachutes during the stripping process (previously discussed); hence, the dynamic-pressure variation from mortar fire to bag stripping was primarily a function of the towing spacecraft and deployment system rather than of parachute characteristics. In the case of the cross parachute, significant inflation occurred prior to bag-stripping (fig. 11) and line-stretch conditions are considered the better basis of comparison. The dynamic pressures for bag stripping are based on estimated times of bag stripping (discussed previouly). Uncertainty of 0.05 second in the time estimate results in 0.1 lb/ft^2 (4.8 N/m^2) uncertainty in dynamic pressure which must be added to the overall uncertainty of approximately 0.5 lb/ft^2 (24 N/m^2) during the deployment sequence. Specific values for the bag-stripping dynamic pressure are given for comparison with line-stretch conditions.

Parachute	Diameter		$q_{\infty,ls}$		$q_{\infty,bs}$	
	ft	m	lb/ft^2	N/m^2	lb/ft^2	N/m^2
Modified ringsail	31.2	9.51	10.8	517	10.5	500
Modified ringsail	54.4	16.6	10.3	493	9.8	461
Disk gap band	30.0	9.14	11.1	531	10.9	522
[1]Disk gap band	40.0	12.2	11.3	541	11.0	527
[2]Disk gap band	40.0	12.2	9.1	436	8.9	424
Disk gap band	64.7	19.7	10.3	493	9.5	455
Cross	30.0	9.14	9.4	450	8.8	421
Cross	54.4	16.6	11.3	541	10.4	496

[1]M_{mf} = 1.91.
[2]M_{mf} = 2.72.

FILLING TIME AND DISTANCE

One parameter of major interest during the deployment sequence is inflation time. Figures 16 and 17 show parachute inflation time divided by nominal parachute diameter as a function of velocity during deployment. The data points shown were obtained from PEPP and SPED I results and supporting ground tests. The curve shown in each figure is an empirical relationship given in reference 24 and altered to represent a geometric porosity of 15 percent. The relationship was established from about 50 tests of various parachutes (mainly ribbon and hyperflow) at velocities ranging from 100 ft/sec (30.0 m/sec) to 2300 ft/sec (701.0 m/sec) and altitudes from 1000 feet (304.8 meters) to 96 500 feet (29 410 meters).

For figure 16, parachute opening time is defined to be the increment between line stretch and full inflation, and deployment velocity is the payload velocity at line stretch. However, when the PEPP results are compared, this method of defining these parameters may not be entirely realistic particularly for the modified-ringsail and disk-gap-band parachutes, because the deployment mortar velocities and stripping distances were

different for each of the tests. In an effort to improve the comparability of the results, parachute inflation time measured from estimated bag stripping to full inflation was calculated. Figure 17 shows the PEPP, SPED I, and supporting tests results obtained by using this definition of filling time. As described previously, all canopies were partially open at time of bag stripping, but neither the modified-ringsail nor the disk-gap-band parachutes had apparently developed significant drag. These data tended to be closer to the empirical relation when the correlation based on bag-stripping time rather than on the line-stretch relationship is applied.

In general, figure 17 shows a better correlation with the empirical curve for the high-altitude – high Mach number data than for the low-speed tests conducted at sea level. However, the high-altitude test at a velocity above 2800 ft/sec (854 m/sec) indicates the possibility of deviation at the higher velocity portion of the curve. Reference 25 also shows such a variation for the higher speed tests and attributes this variation to a possible flow-field change around the canopy at a given velocity. For the parachutes tested in the PEPP and SPED I program, it may be that a significant flow-field change occurs at velocities near 2000 ft/sec (610 m/sec) and thus results in the possible divergence between the empirical relationship and the flight data at higher velocities.

Figures 18 and 19 show the total distances traveled by the parachute systems during inflation in terms of nominal diameter as a function of velocity. In figure 18, the inflation distance is measured between line stretch and full inflation whereas the velocity is that at line stretch. Figure 19 shows the distance traveled beginning at the time of estimated bag stripping. Both figures show a possible trend of increasing inflation distance with increased velocity. The possible effects of atmospheric density and Mach number cannot be determined until more tests are available.

CANOPY STABILITY

Histories of the canopy projected area for the three types of parachutes deployed at Mach numbers near 1.6 from the balloon-launched tests are shown in figure 20. These histories were obtained by cameras looking at the parachute from the attached payload. All three types of parachutes exhibited a partial collapse and subsequent re-inflation immediately after the instant of first full inflation. The amount of partial collapse was least for the modified-ringsail and most for the disk-gap-band parachutes. Both the modified-ringsail and disk-gap-band configurations subsequently attained a stable inflation condition when the canopy appeared tight and rigid whereas the cross-type configuration did not. The panels of the cross parachute exhibited a "scissoring" motion which appeared to amplify initially and thus prevented a stable condition from being achieved during the data period. The rocket-launched tests of each configuration in smaller sizes at similar Mach numbers (refs. 3, 4, and 6) exhibited nearly the identical characteristics

of the larger parachutes. The degree of canopy fluctuations for the cross parachute was much less on the smaller scale than the large-size test. The fact that the smaller scale parachutes were of somewhat heavier (and probably more rigid) construction may account for at least part of these observed differences in canopy stability characteristics.

When the deployment Mach number was increased, a reduction in the canopy stability was observed. The disk-gap-band configuration was deployed at Mach numbers as high as 2.72 (full inflation occurred at a Mach number of 2.67). Figure 21 (taken from ref. 12) shows the projected-area history for this test. Partial collapse and subsequent re-inflation, as described previously, were evident, but the canopy did not achieve a stable condition until the Mach number was below 1.4. The test which deployed a similar configuration at a Mach number of 1.91 (ref. 11) also showed some unsteadiness until the lower supersonic Mach numbers were reached. No tests were conducted of either the modified-ringsail or cross configurations to determine their behavior at Mach numbers above 1.6. It is also not known whether the high-velocity fluctuations could be corrected by minor canopy or geometric porosity changes in the disk-gap-band design. Despite the canopy fluctuations, the disk-gap-band configuration produced good deceleration characteristics at the higher Mach numbers.

DRAG CHARACTERISTICS

Tensiometer, accelerometer, and trajectory data were used to calculate the force coefficient (essentially the drag coefficient $C_{D,o}$) during trajectory ascent immediately following parachute inflation. Near apogee, drag coefficients were not obtained because of large inaccuracies caused by the combination of low dynamic pressures and trajectory uncertainty. After apogee, trajectory data were used to determine the effective drag coefficient $(C_{D,o})_{eff}$ which is the drag coefficient based on vertical velocity and acceleration during descent. Both the high Mach number drag coefficients prior to apogee and the low Mach number effective drag coefficients during descent are shown in figures 22 to 24. The data are presented in terms of envelopes which enclose both scatter and oscillations. Significant oscillations shortly after first full inflation were preserved when fairing the envelopes. Arbitrary faired curves were drawn through the envelopes for ease of comparison.

Figure 22 shows results obtained from the tests of the modified-ringsail configuration. Values presented for the 85.3-foot-diameter (26-meter) test should be viewed with caution because of the excessive permeability of the canopy cloth for that particular parachute. Figure 23 presents drag coefficient characteristics of the disk-gap-band configuration. An apparent loss in drag as a result of projected-area variation immediately after first full inflation is characteristic of all tests. In the test where inflation occurred near Mach 2.67, the drag continued to oscillate significantly after the post-inflation loss.

Steady results consistent with the other tests were beginning to be achieved by the time the system reached Mach 1.45. The probable cause for the large oscillations is the elastic characteristics of the suspension lines being amplified by the canopy instability in a low-density environment. (See ref. 12.) The faired curve for the supersonic envelope is based only on trajectory data in this case. Data below Mach 1.45 for $C_{D,o}$ were omitted because of inaccuracies associated with trajectory apogee. Figure 24 shows drag coefficients for the cross parachutes. The $C_{D,o}$ amplitudes are somewhat proportional to the projected-area variations which were different for the two parachutes. As stated previously, the 30.0-foot (9.14-meter) configuration was of heavier construction (and probably less flexible) than the larger parachute. As described in reference 10, canopy motions for the 54.4-foot (16.6-meter) configuration were very large after apogee during descent. The oscillations do not appear in the effective drag coefficient envelope because these calculations were based on smoothed velocity data. The 30.0-foot (9.14-meter) canopy exhibited significantly lower fluctuation amplitudes during descent than the larger configuration did.

Comparison of the faired drag coefficient curves is shown in figure 25. The faired curves are inconsistent during the period immediately following first full inflation for all parachute types. Once canopy fluctuations and longitudinal oscillations disappear, drag coefficient is nearly constant over the Mach number range of these tests. The cross parachute has the highest drag coefficient values. Part of this advantage however is caused by the different definitions of the reference area. If all parachute types used only the cloth area as the reference area, the advantage of the cross parachute would not be as great as indicated in figure 25.

Figure 26 shows $(C_{D,o})_{eff}$ during descent as a function of canopy size. Also indicated is the geometric porosity λ_g and permeability λ_m associated with the various test parachutes. Permeability was very low for both cross parachutes. The exact influence of permeability at high altitudes is unknown; however, it is expected that the difference between the values for the two cross parachutes had little influence on performance during descent. It is believed that the principal causes of the larger $(C_{D,o})_{eff}$ values for the 54-foot (16.6-meter) canopy were fluctuation (scissoring) characteristics or size effects. Reynolds number effects are not believed to be important because drag coefficients do not vary over wide Reynolds number ranges for most parachutes. (See ref. 20.) In the case of the modified-ringsail configuration, the 85.3-foot-parachute (26-meter) data must be viewed with caution because of the excessive permeability of that canopy. (See ref. 5.) The increased value of $(C_{D,o})_{eff}$ for the 54.5-foot (16.6-meter) configuration over the 31.2-foot (9.51-meter) parachute is probably associated with size effects and differences in canopy configuration. Similar increases in drag coefficient with size for ringsail parachutes have been observed in reference 21.

Size effects appear to be a minimum for the disk-gap-band configuration when the probable effect of geometric porosity is taken into account. The exact influence of the high permeability material used in the band on the 64.7-foot (19.7-meter) configuration however is unknown.

CONCLUDING REMARKS

A limited number of flight tests of modified-ringsail, disk-gap-band, and cross parachute configurations have been conducted. The data from these tests are described herein and further tests would be required to establish repeatability. However, comparison of the available flight results indicates that the following general remarks can be made:

1. Snatch force values calculated by an existing theoretical method were not exceeded by flight results probably because of the mechanism of deployment used in these tests.

2. Comparison of opening-force parameters based on dynamic pressure near full inflation showed no definite trend with Mach number.

3. Ground-track photographs of the inflation process showed that neither the modified-ringsail nor the disk-gap-band canopies inflated significantly prior to completion of the deployment bag stripping from the canopy. The cross parachute however did experience significant inflation prior to completion of bag stripping.

4. Correlation of filling times from estimated time of bag stripping to time of full inflation showed good agreement with empirically derived curves.

5. All parachutes were characterized by a partial collapse and fluctuations of the canopy immediately after the first inflation peak. The partial collapse was most severe for the disk-gap-band configuration and least severe for the modified-ringsail system.

6. The cross parachute never achieved a stable configuration during the data periods and was characterized by a scissoring motion. Both the modified-ringsail and disk-gap-band systems were stable for Mach numbers below 1.4 once deployment dynamic effects had diminished.

7. Even though the canopies of the cross and disk-gap-band (at high Mach numbers) configurations exhibited fluctuations, both systems were good drag-producing devices.

8. Comparison of drag coefficients indicates the cross configuration produced the highest values even if all values are based on cloth area alone. Generally, the drag coefficients of the modified-ringsail configuration were slightly higher than those for the disk-gap-band systems.

Langley Research Center,
National Aeronautics and Space Administration,
Langley Station, Hampton, Va., April 14, 1969,
709-08-00-01-23.

APPENDIX

ESTIMATES OF DEPLOYMENT BAG VELOCITY AT MORTAR-FIRE AND LINE-STRETCH CONDITIONS

The velocities of the deployment bag at mortar fire and line stretch were not directly measured on the PEPP and SPED I flights. These quantities may be estimated based on the following conditions.

At the first instant after mortar fire, the exit velocity of the deployment bag relative to the towing spacecraft equals $V_{R,mf}$. At the instant of line stretch, the relative velocity between the spacecraft and deployment bag is

$$V_{R,ls} = V_{R,mf} - \Delta V_v + \overline{\dot{V}}_b \Delta t \tag{A1}$$

The average relative velocity during the period from mortar fire to line stretch is

$$\overline{V}_R = \frac{2V_{R,mf} - \Delta V_v + \overline{\dot{V}}_b \Delta t}{2} \tag{A2}$$

Rearranging equation (A2) yields

$$V_{R,mf} = \frac{2\overline{V}_R + \Delta V_v - \overline{\dot{V}}_b \Delta t}{2} \tag{A3}$$

by assuming that drag is the principal force acting on the bag during line stretching, and then considering only longitudinal motion

$$\overline{\dot{V}}_b \approx \frac{\overline{-(C_D S)_b q_w} + g \sin \gamma}{\overline{m}_b} \tag{A4}$$

Then $V_{R,mf}$ is estimated from

$$V_{R,mf} = \frac{2\overline{V}_R + \Delta V_v - \left[\dfrac{\overline{-(C_D S)_b q_w} + g \sin \gamma}{\overline{m}_b}\right] \Delta t}{2} \tag{A5}$$

and $V_{R,ls}$ is

$$V_{R,ls} = V_{R,mf} - \Delta V_V + \frac{\overline{-(C_D S)_b q_w} + g \sin \gamma}{\overline{m}_b} \Delta t \qquad \text{(A6)}$$

The quantity $\overline{V}_R$ is obtained from flight results if the times of mortar fire and line stretch, and the lengths of the suspension lines and bridle are known. The term ΔV_V is available from flight trajectory data based on integration of accelerometer records. Values for γ and Δt are available from flight trajectory results, and $\overline{m}_b$ is estimated based on the packed parachute – deployment bag (and mortar lid) system with 50 percent of the suspension lines contained within the system. The quantity $(C_D S)_b$ was assumed to be 0.94 for the 1 foot-diameter deployment bag system. The quantity q_w was assumed to be 50 percent of the free-stream dynamic pressure at mortar fire to take into account probable wake degradation, time gradients, and longitudinal displacement gradients for the balloon-launched tests; 90 percent was used for the rocket-launched results because of lesser probable dynamic pressure gradients and wake effects. The values calculated from the flight results are as follows:

Parachute	Diameter		Nominal $V_{R,mf}$		Flight $V_{R,mf}$		Flight $V_{R,ls}$	
	ft	m	fps	mps	fps	mps	fps	mps
Modified ringsail	31.2	9.51	120	37	108	32.9	115	35.1
Modified ringsail	40.0	12.2	120	37	111	33.8	117	37.7
Disk gap band	30.0	9.14	120	37	109	33.2	115	35.1
Disk gap band $(M_{mf} = 1.91)$	40.0	12.2	120	37	118	36.0	123	37.5
Disk gap band $(M_{mf} = 2.72)$	40.0	12.2	120	37	109	33.2	115	35.1
Cross	30.0	9.14	120	37	113	34.4	120	36.6
Modified ringsail	85.3	26.0	130	40	146	44.5	123	37.5
Modified ringsail	54.5	16.6	130	40	139	42.4	94	28.7
Disk gap band	64.7	19.7	130	40	138	42.1	106	32.3
Cross	54.4	16.6	130	40	147	44.8	87	26.5

Uncertainties in the calculated values are ±5 fps based on the root sum square of deviations caused by errors of ±10 fps in ΔV_V, ±2 fps in V_R, and 30-percent error in $\overline{(C_D S)_b q_w}$.

For the rocket-launched tests, the estimated flight values of $V_{R,mf}$ are somewhat lower than the nominal values of 120 fps. This difference is due to the fact that part of the energy was absorbed in accelerating the towing spacecraft to a higher velocity (between 10 and 20 fps), and $V_{R,mf}$ is relative to the spacecraft velocity at the initiation of mortar fire prior to the velocity increase. In the case of the balloon tests, flight values of $V_{R,mf}$ are somewhat higher than the nominal 130 fps. The mortar in this

case did not produce a significant velocity increase because of heavier spacecraft weights than the rocket-launched tests. Within each series of tests, the scatter in the flight values of $V_{R,mf}$ is typical of that experienced during prelaunch ground tests of the mortar systems.

For the rocket-launched tests, the estimated values show an increase in deployment-bag velocity relative to the spacecraft between the times of mortar fire and line stretch. This increase is probably due to the m/C_DS of the towing spacecraft being about 4 whereas the m/C_DS of the bag was near 1.

For the balloon-launched tests, the estimated values show a decrease in relative velocity. This decrease is probably due to the m/C_DS of the spacecraft being about 0.15 whereas the m/C_DS of the bag was about 1 and also due to possible wake effects.

REFERENCES

1. Gillis, Clarence L.; and Bendura, Richard J.: Full-Scale Simulation of Parachute Deployment Environment in the Atmosphere of Mars. 14th Annual Technical Meeting Proceedings, Inst. Environ. Sci., 1968, pp. 469-475.

2. McFall, John C., Jr.; and Murrow, Harold N.: Parachute Testing at Altitudes Between 30 and 90 Kilometers. J. Spacecraft Rockets (Eng. Notes), vol. 4, no. 6, June 1967, pp. 796-798.

3. Preisser, John S.; Eckstrom, Clinton V.; and Murrow, Harold N.: Flight Test of a 31.2-Foot-Diameter Modified Ringsail Parachute Deployed at a Mach Number of 1.39 and a Dynamic Pressure of 11.0 Pounds Per Square Foot. NASA TM X-1414, 1967.

4. Eckstrom, Clinton V.; and Preisser, John S.: Flight Test of a 30-Foot-Nominal-Diameter Disk-Gap-Band Parachute Deployed at a Mach Number of 1.56 and a Dynamic Pressure of 11.4 Pounds Per Square Foot. NASA TM X-1451, 1967.

5. Eckstrom, Clinton, V.; Murrow, Harold N.; and Preisser, John S.: Flight Test of a 40-Foot-Nominal-Diameter Modified Ringsail Parachute Deployed at a Mach Number of 1.64 and a Dynamic Pressure of 9.1 Pounds Per Square Foot. NASA TM X-1484, 1967.

6. Preisser, John S.; and Eckstrom, Clinton V.: Flight Test of a 30-Foot-Nominal-Diameter Cross Parachute Deployed at a Mach Number of 1.57 and a Dynamic Pressure of 9.7 Pounds per Square Foot. NASA TM X-1542, 1968.

7. Whitlock, Charles H.; Bendura, Richard J.; and Coltrane, Lucille C.: Performance of a 26-Meter-Diameter Ringsail Parachute in a Simulated Martian Environment. NASA TM X-1356, 1967.

8. Bendura, Richard J.; Huckins, Earle K., III; and Coltrane, Lucille C.: Performance of a 19.7-Meter-Diameter Disk-Gap-Band Parachute in a Simulated Martian Environment. NASA TM X-1499, 1968.

9. Whitlock, Charles H.; Henning, Allen B.; and Coltrane, Lucille C.: Performance of a 16.6-Meter-Diameter Modified Ringsail Parachute in a Simulated Martian Environment. NASA TM X-1500, 1968.

10. Lundstrom, Reginald R.; Darnell, Wayne L., and Coltrane, Lucille C.: Performance of a 16.6-Meter-Diameter Cross Parachute in a Simulated Martian Environment. NASA TM X-1543, 1968.

11. Preisser, John S.; and Eckstrom, Clinton V.: Flight Test of a 40-Foot-Nominal-Diameter Disk-Gap-Band Parachute Deployed at a Mach Number of 1.91 and a Dynamic Pressure of 11.6 Pounds per Square Foot. NASA TM X-1575, 1968.

12. Eckstrom, Clinton V.; and Preisser, John S.: Flight Test of a 40-Foot-Nominal-Diameter Disk-Gap-Band Parachute Deployed at a Mach Number of 2.72 and a Dynamic Pressure of 9.7 Pounds Per Square Foot. NASA TM X-1623, 1968.

13. Mayhue, Robert J.; and Eckstrom, Clinton V.: Flight-Test Results From Supersonic Deployment of an 18-Foot-Diameter (5.49-Meter) Towed Ballute Decelerator. NASA TM X-1773, 1969.

14. Stone, F. J.: 40-Ft-Diameter Ringsail Parachute. PEPP Rep. PR25-35 R/L-5, Pioneer Parachute Co., Inc.

15. Lemke, Reinhold: 40-Ft DGB Parachute. PEPP Rep. PR25-36 SPED-I, G. T. Schjeldahl Co., Oct. 13, 1967.

16. Stone, F. J.: 55-ft-D_o Ringsail Parachute. PEPP Rep. PR25-33 B/L-3, Pioneer Parachute Co., Inc., Dec. 1967.

17. Lemke, Reinhold A.; and Niccum, Ronald J.: 65-Foot Diameter D-G-B Parachute. PEPP Rep. PR25-32 B/L-2, G. T. Schjeldahl Co., July 14, 1967.

18. Boettcher, E. W.; and Hanson, G. P.: Cross Parachute. PEPP Rep. PR25-34 B/L-4, Raven Industries, Inc.

19. Darnell, Wayne L.; Henning, Allen B.; and Lundstrom, Reginald R.: Flight Test of a 15-Foot Diameter (4.6 Meter) 120^{o} Conical Spacecraft Simulating Parachute Deployment in a Mars Atmosphere. NASA TN D-4266, 1967.

20. Anon.: Performance of and Design Criteria for Deployable Aerodynamic Decelerators. ASD-TR-61-579, U.S. Air Force, Dec. 1963.

21. Ewing, E. G.: Development Program for a Ringsail Parachute. NVR 5028, Northrop Corp., Dec. 1966.

22. French, Kenneth E.: Comment on "A Method for Calculating Parachute Opening Forces for General Deployment Conditions." J. Spacecraft Rockets (Tech. Comments), vol. 4, no. 10, Oct. 1967, pp. 1407-1408.

23. French, Kenneth E.: Model Law for Parachute Opening Shock. AIAA J., vol 2, no. 12 Dec. 1964, pp. 2226-2228.

24. Fredette, R. O.: Parachute Research Above Critical Aerodynamic Velocities. P-1031C, Cook Res. Labs., Cook Electric Co., c.1961.

25. Berndt, R. J.: and Deweese, J. H.: Filling Time Prediction Approach for Solid Cloth Type Parachute Canopies. AIAA Aerodynamic Deceleration Systems Conference, Sept. 1966, pp. 17-32.

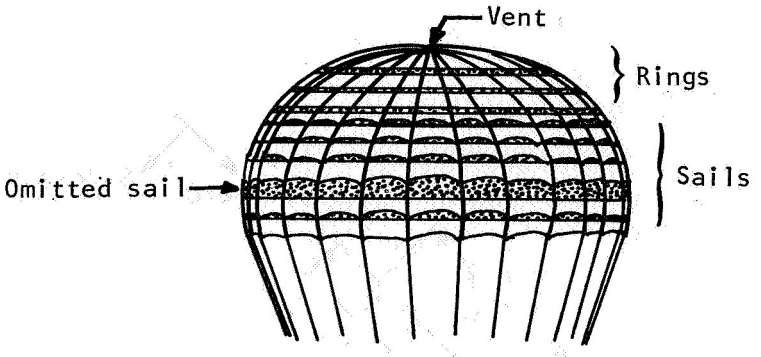

(a) Modified ringsail.

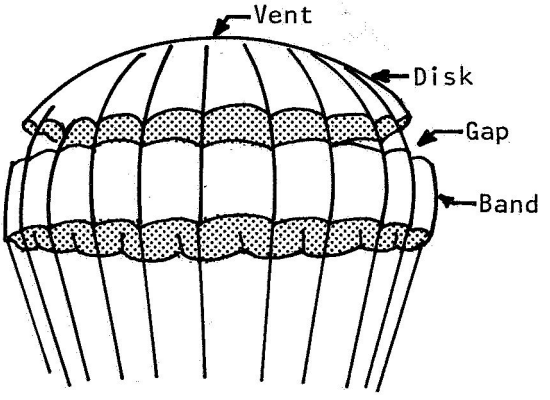

(b) Disk gap band.

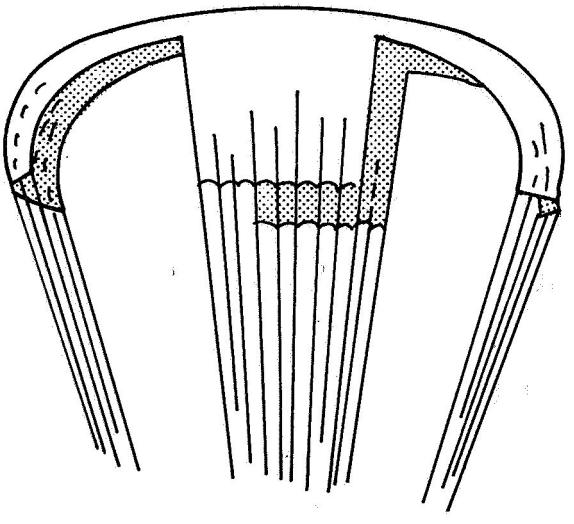

(c) Cross.

Figure 1.- Parachute configurations.

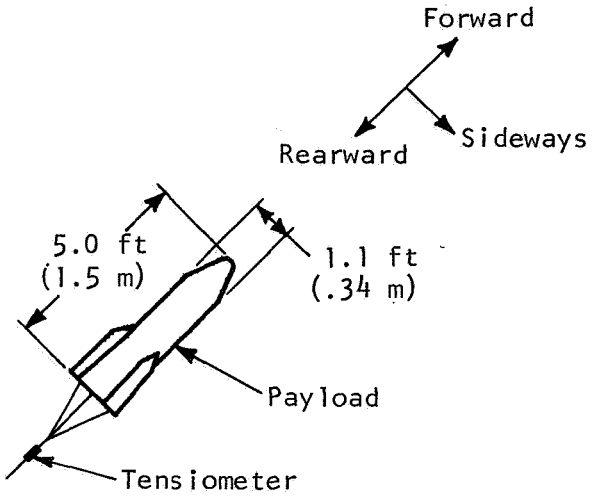

(a) Rocket-launched system.

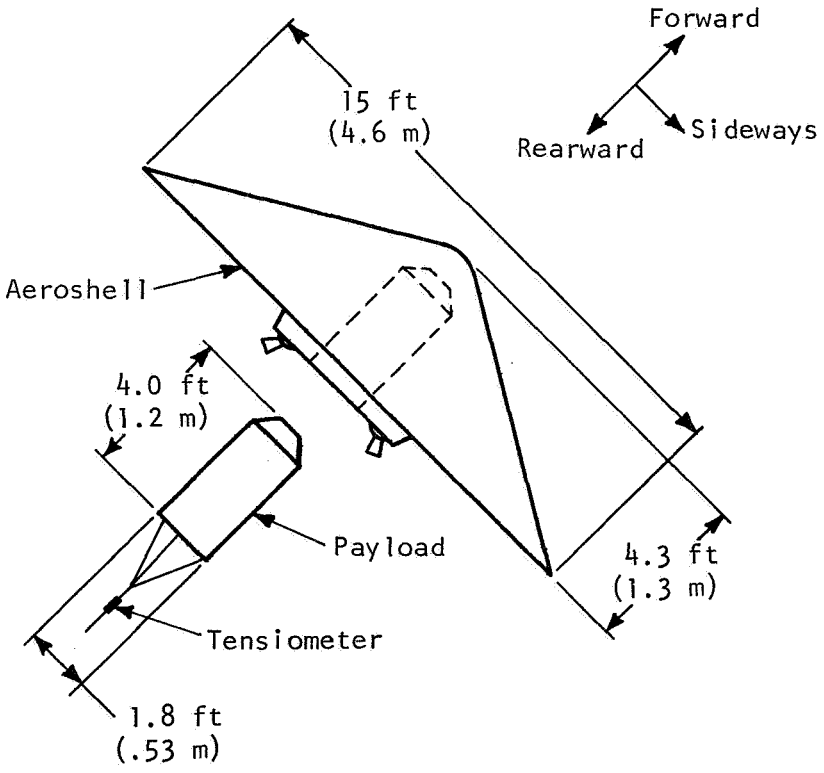

(b) Balloon-launched system.

Figure 2.- Sketch of payload configurations.

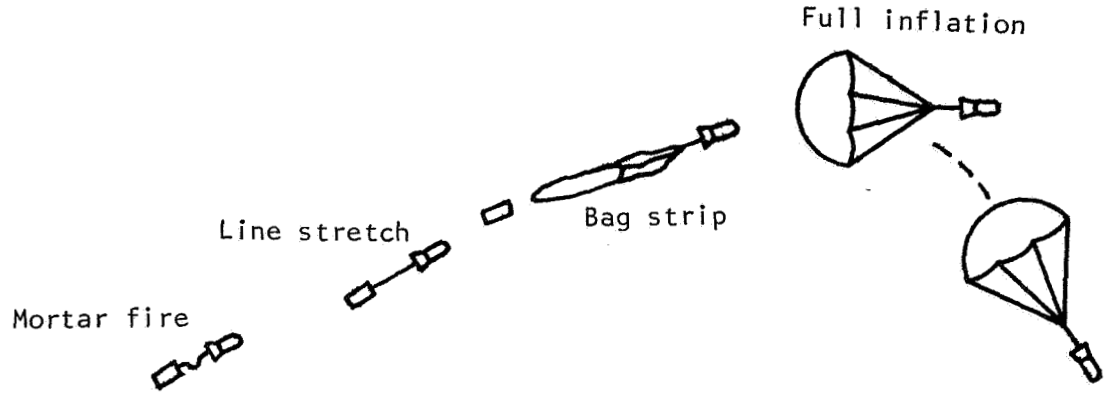

(a) Rocket-launched tests.

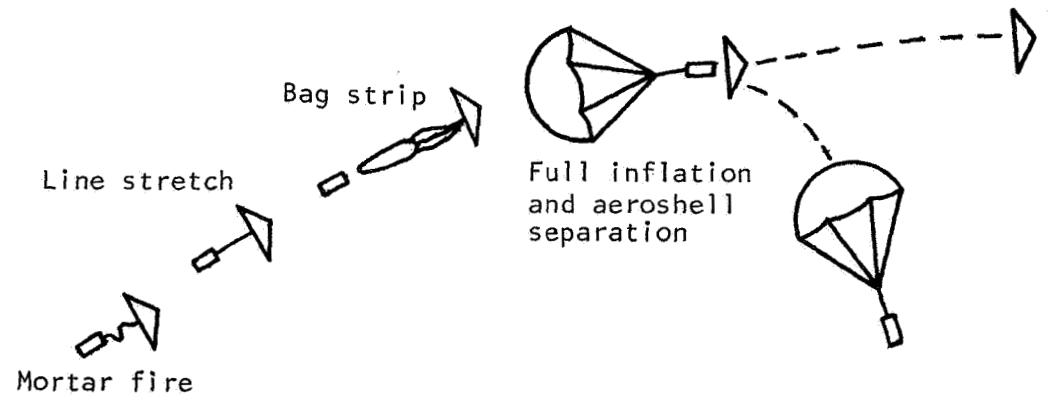

(b) Balloon-launched tests.

Figure 3.- Deployment sequence.

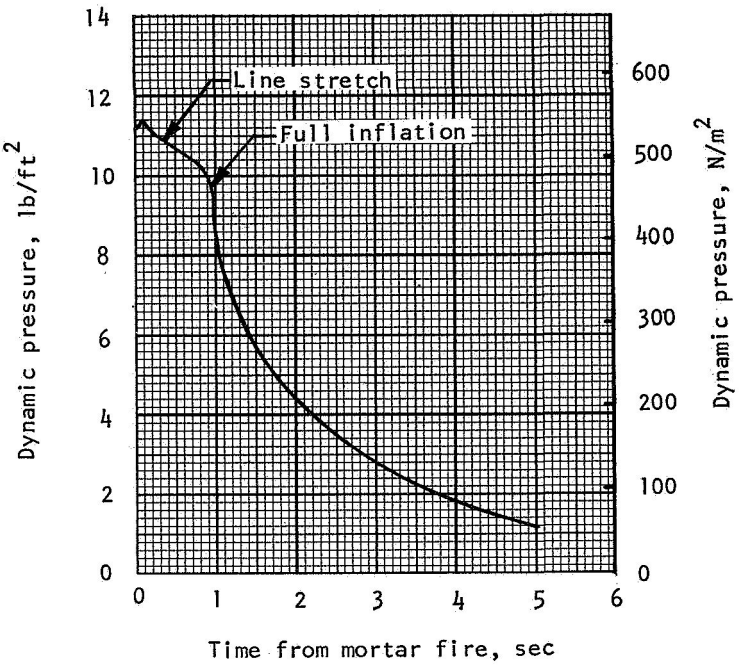

(a) Rocket-launched 30.0-foot (9.14-meter) disk-gap-band test.

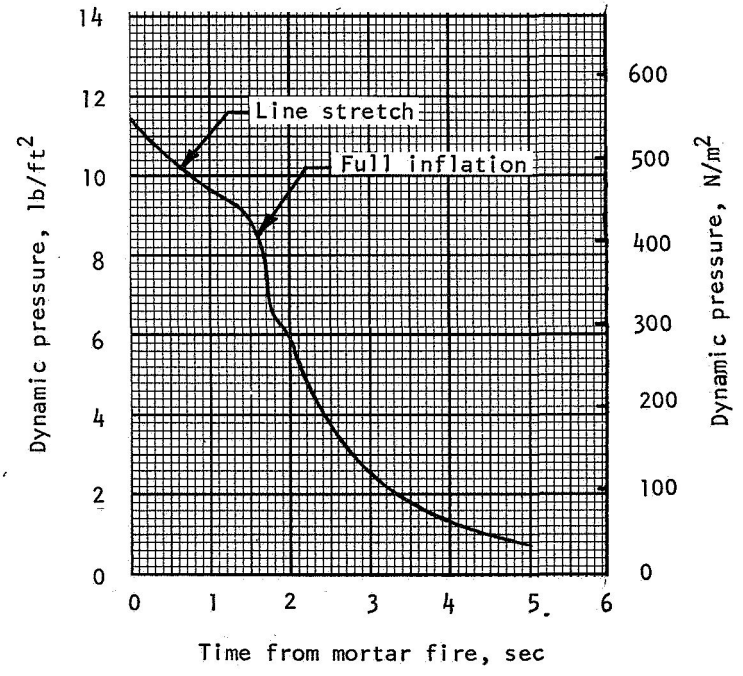

(b) Balloon-launched 64.7-foot (19.7-meter) disk-gap-band test.

Figure 4.- Typical dynamic-pressure time histories.

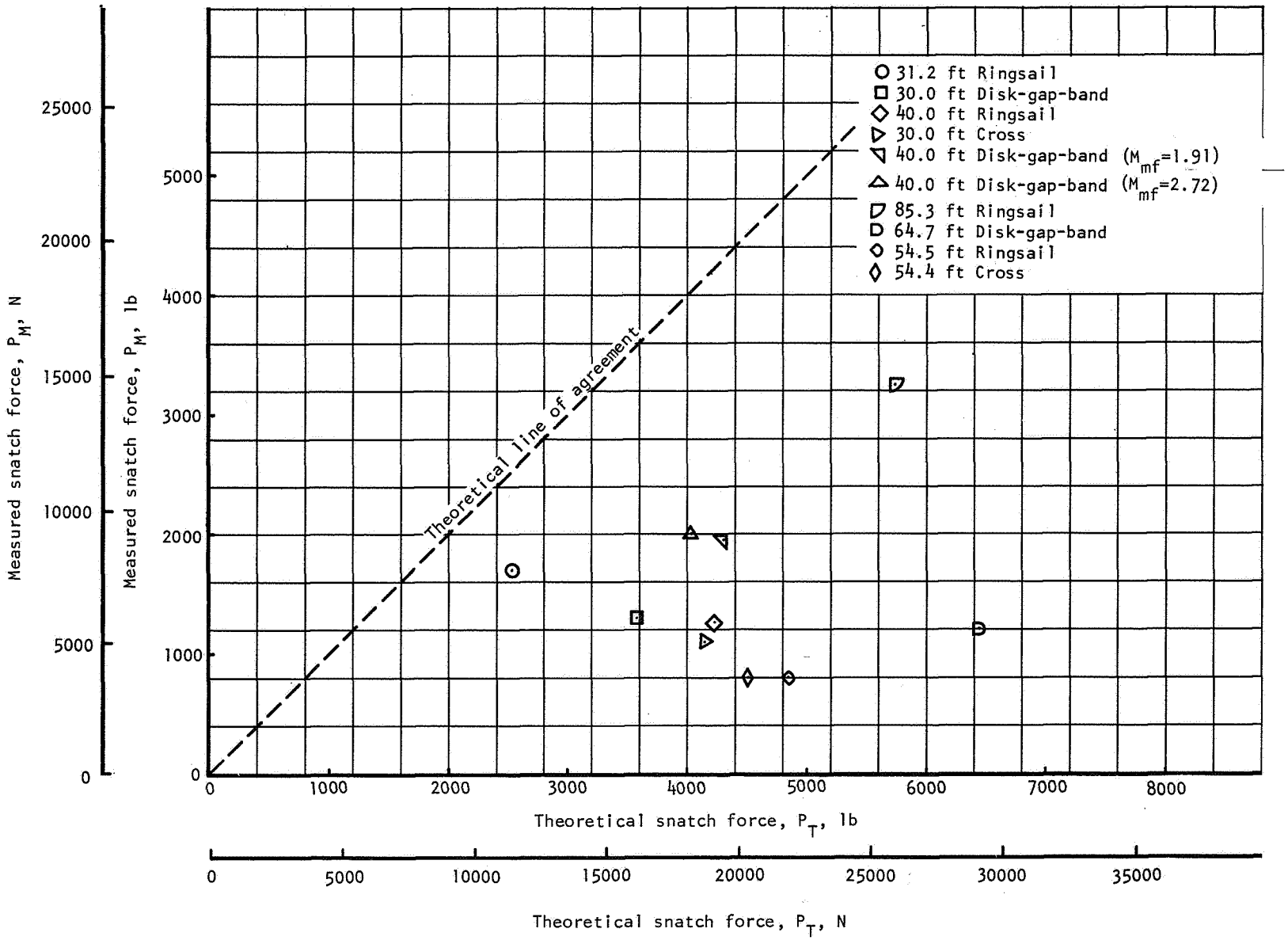

Figure 5.- Comparison of actual and theoretical snatch forces. (1 foot = 0.3048 meter.)

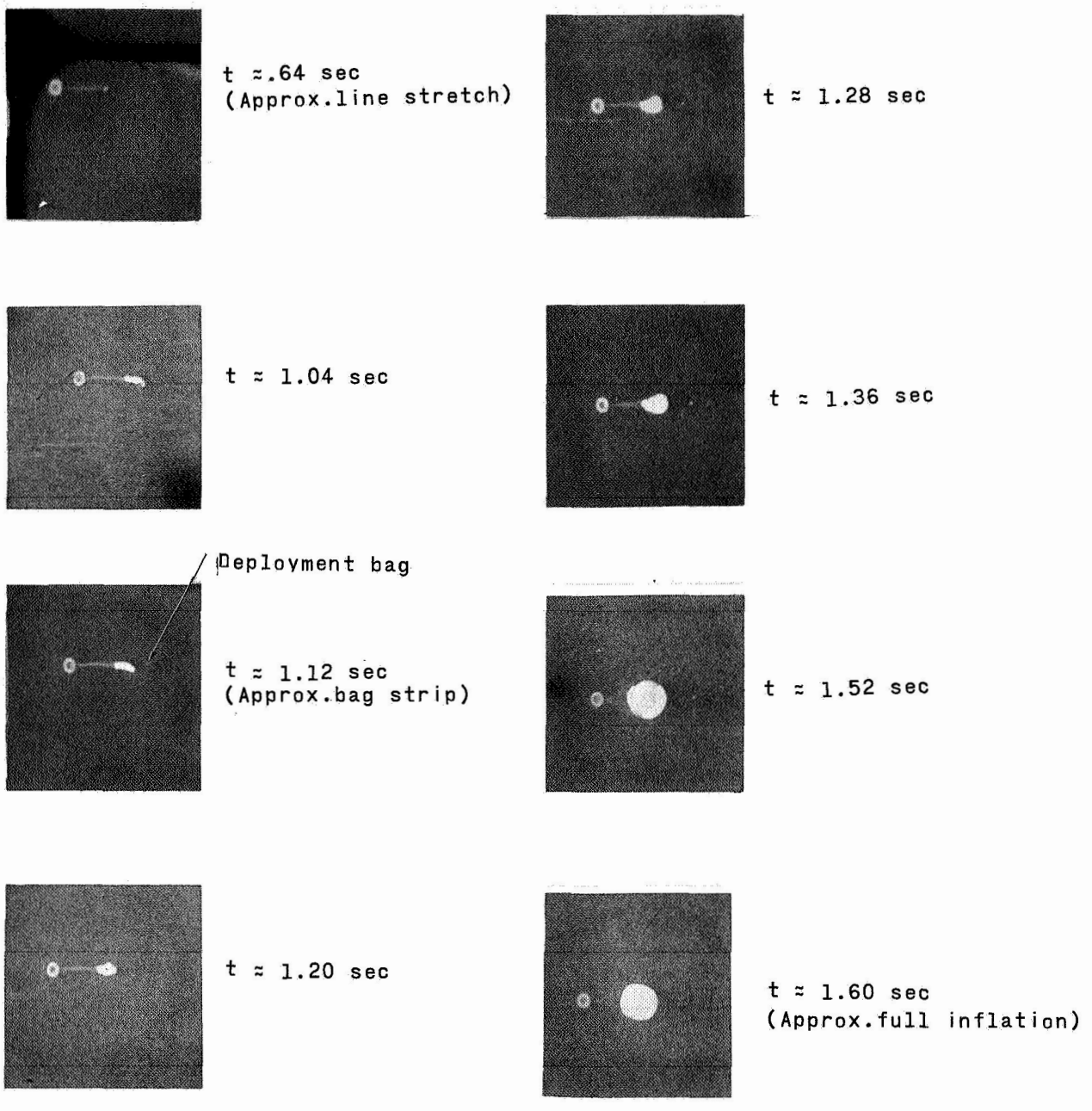

L-69-1354

Figure 6.- Selected frames from ground-based cameras of 64.7-foot (19.7-meter) disk-gap-band parachute test.

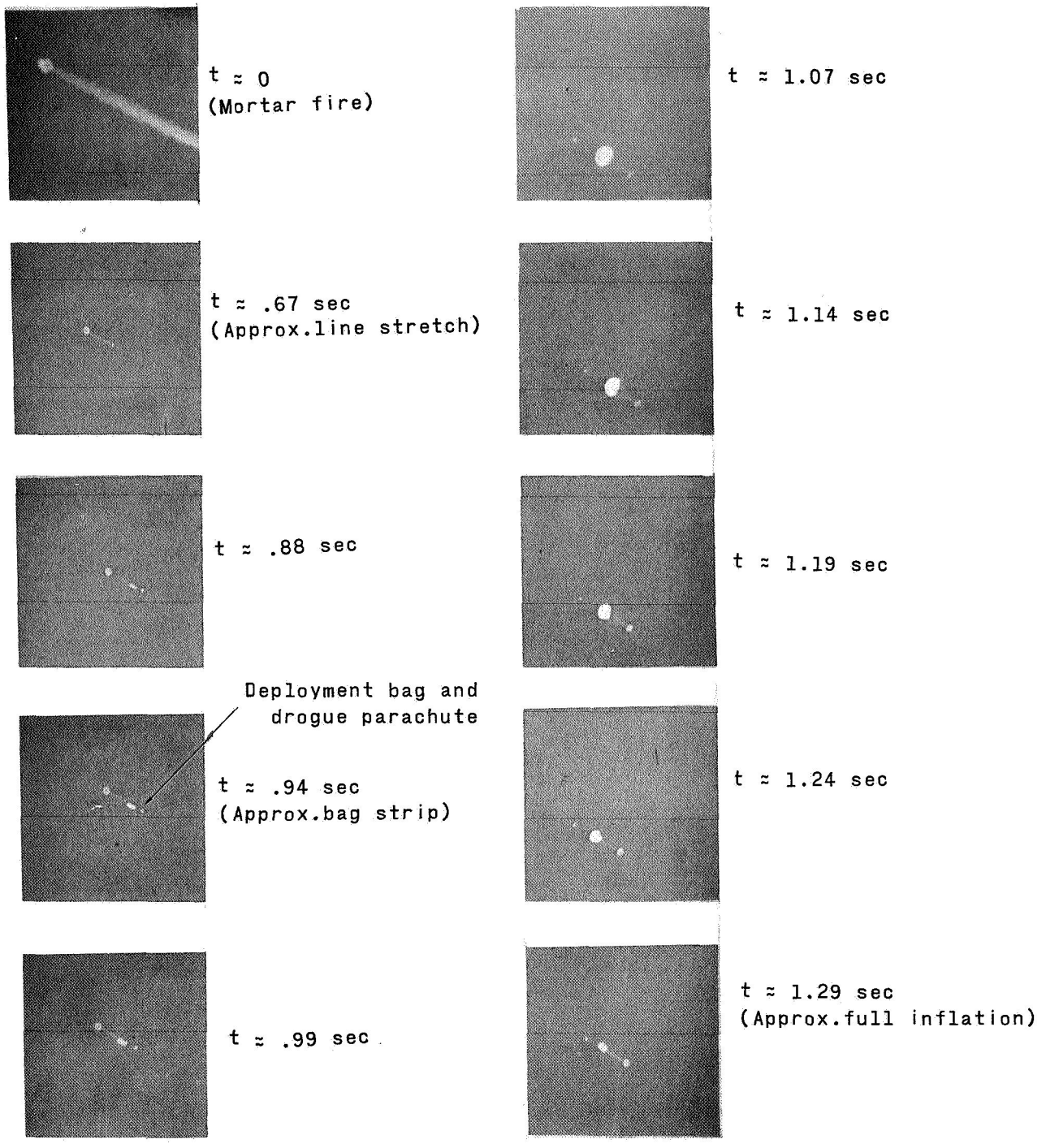

L-69-1355

Figure 7.- Selected frames from ground-based cameras of 54.5-foot (16.6-meter) modified ringsail parachute test.

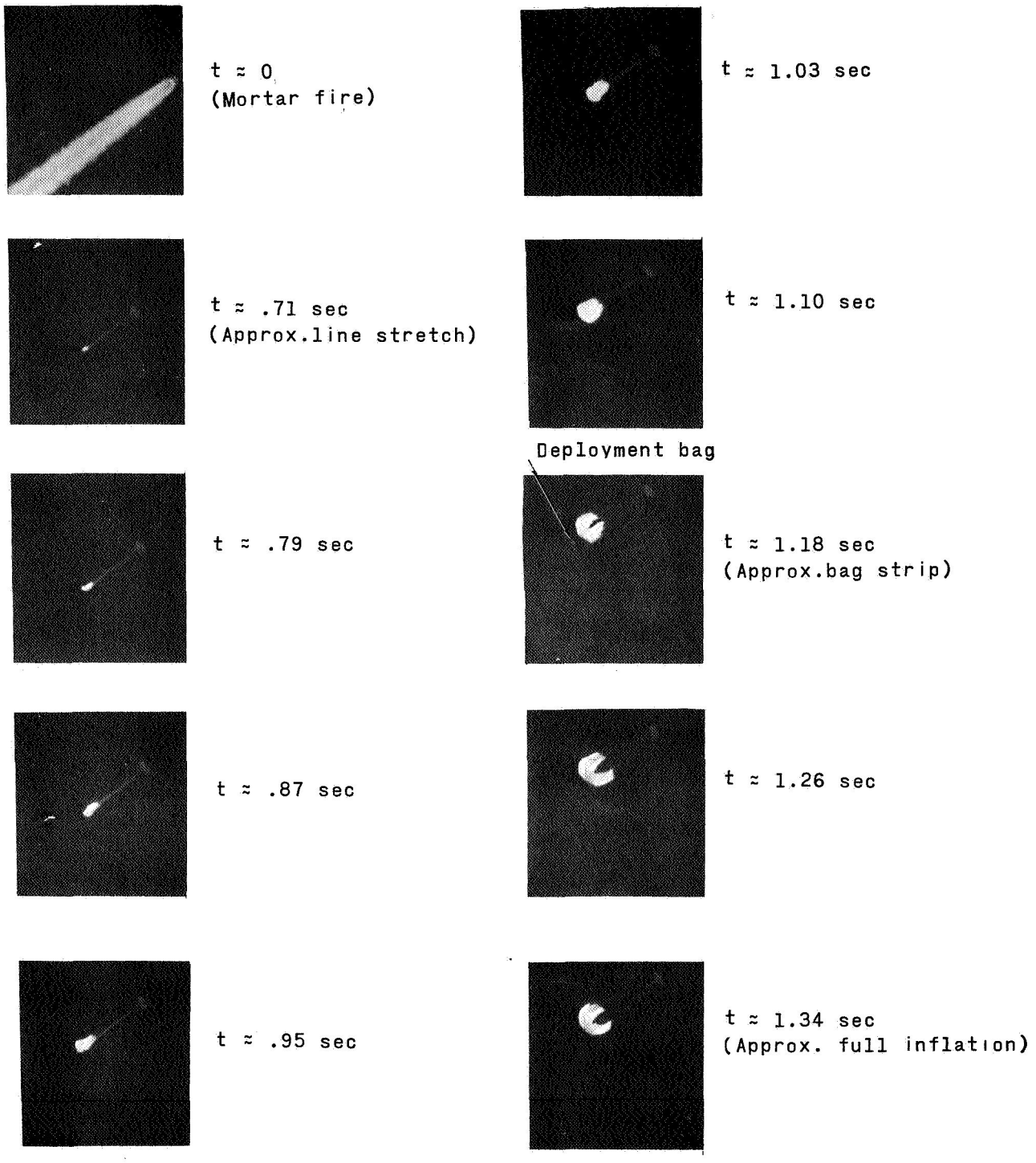

L-69-1356

Figure 8.- Selected frames from ground-based cameras of 54.4-foot (16.6-meter) cross parachute test.

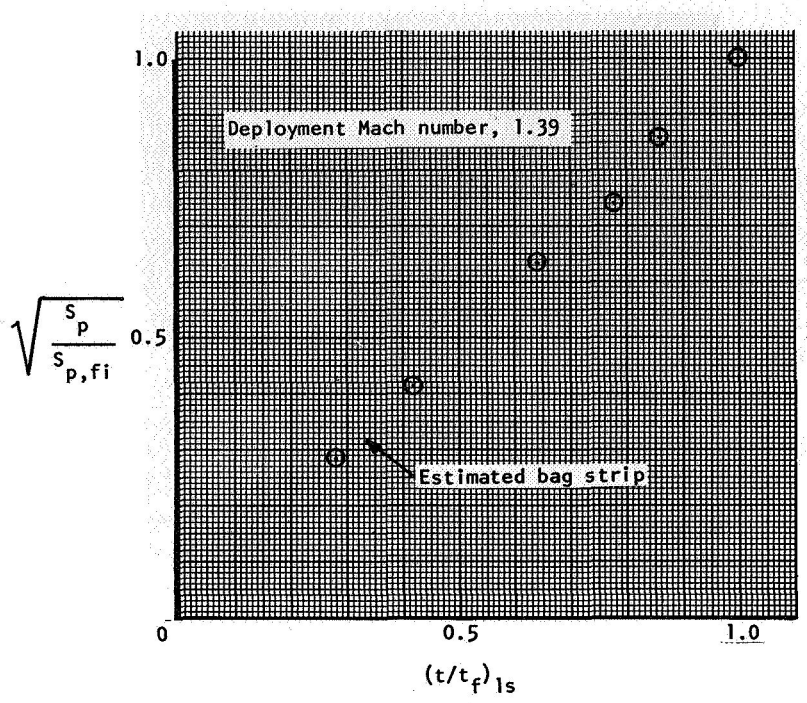

(a) D_0 = 31.2 feet (9.51 meters).

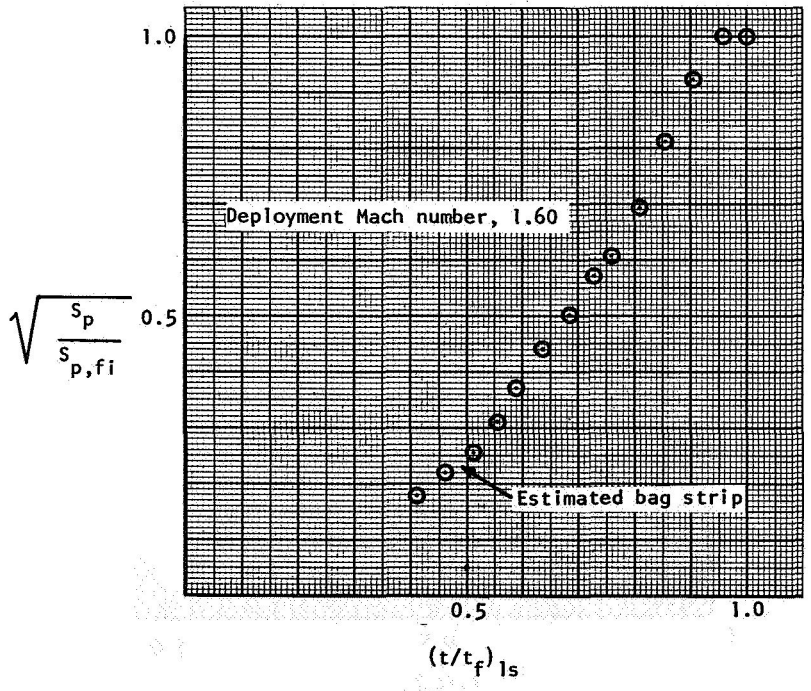

(b) D_0 = 54.5 feet (16.6 meters).

Figure 9.- Canopy growth parameter history for modified-ringsail parachutes.

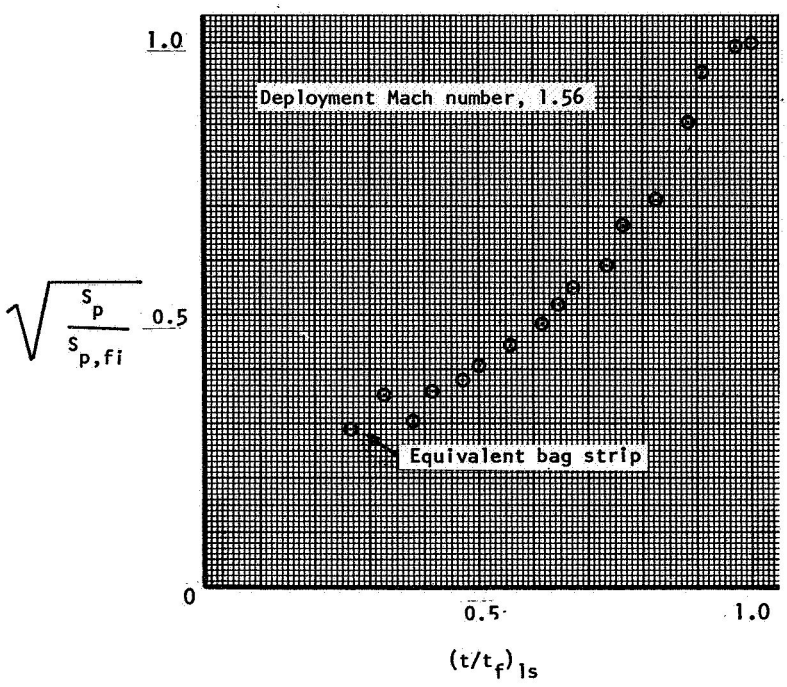

(a) D_0 = 30.0 feet (9.14 meters).

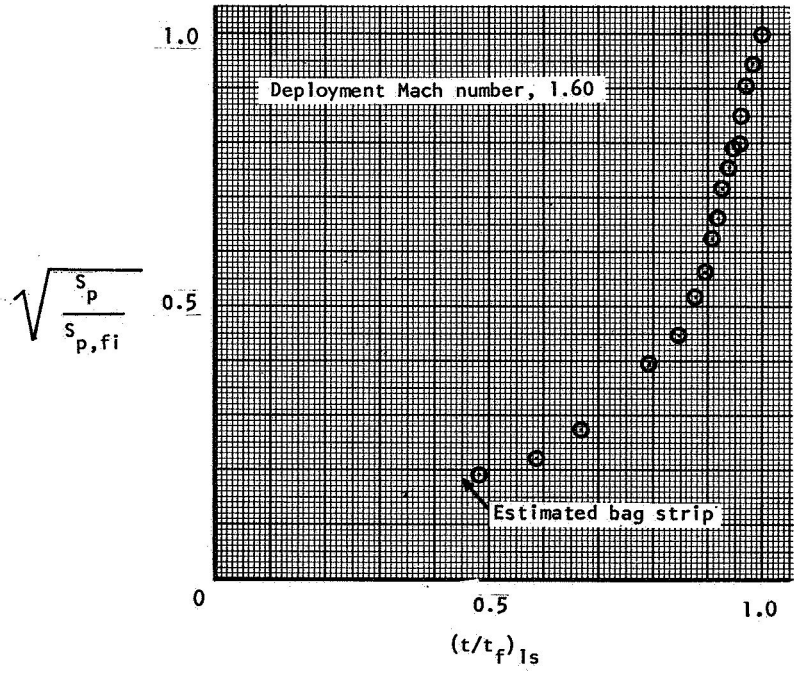

(b) D_0 = 64.7 feet (19.7 meters).

Figure 10.- Canopy growth parameter history for disk-gap-band parachutes.

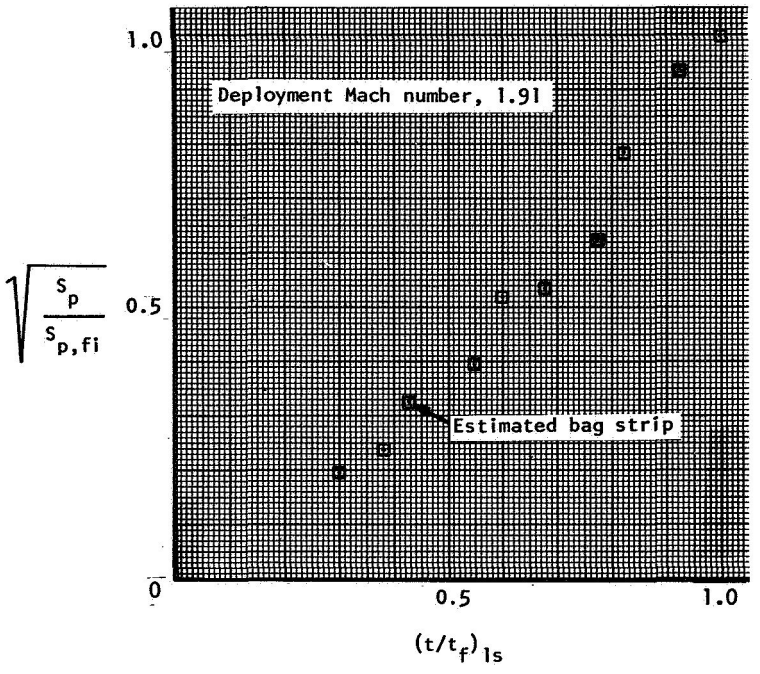

(c) D_0 = 40.0 feet (12.2 meters).

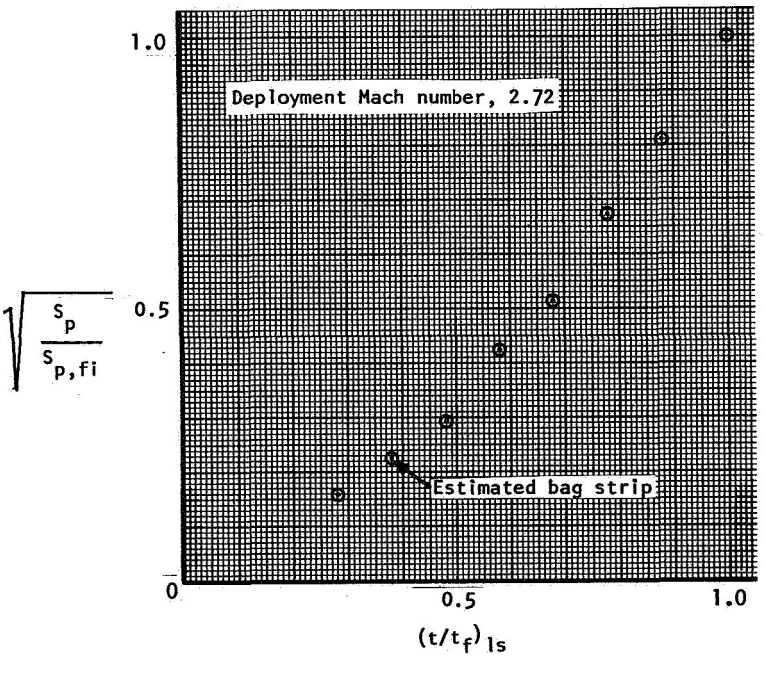

(d) D_0 = 40.0 feet (12.2 meters).

Figure 10.- Concluded.

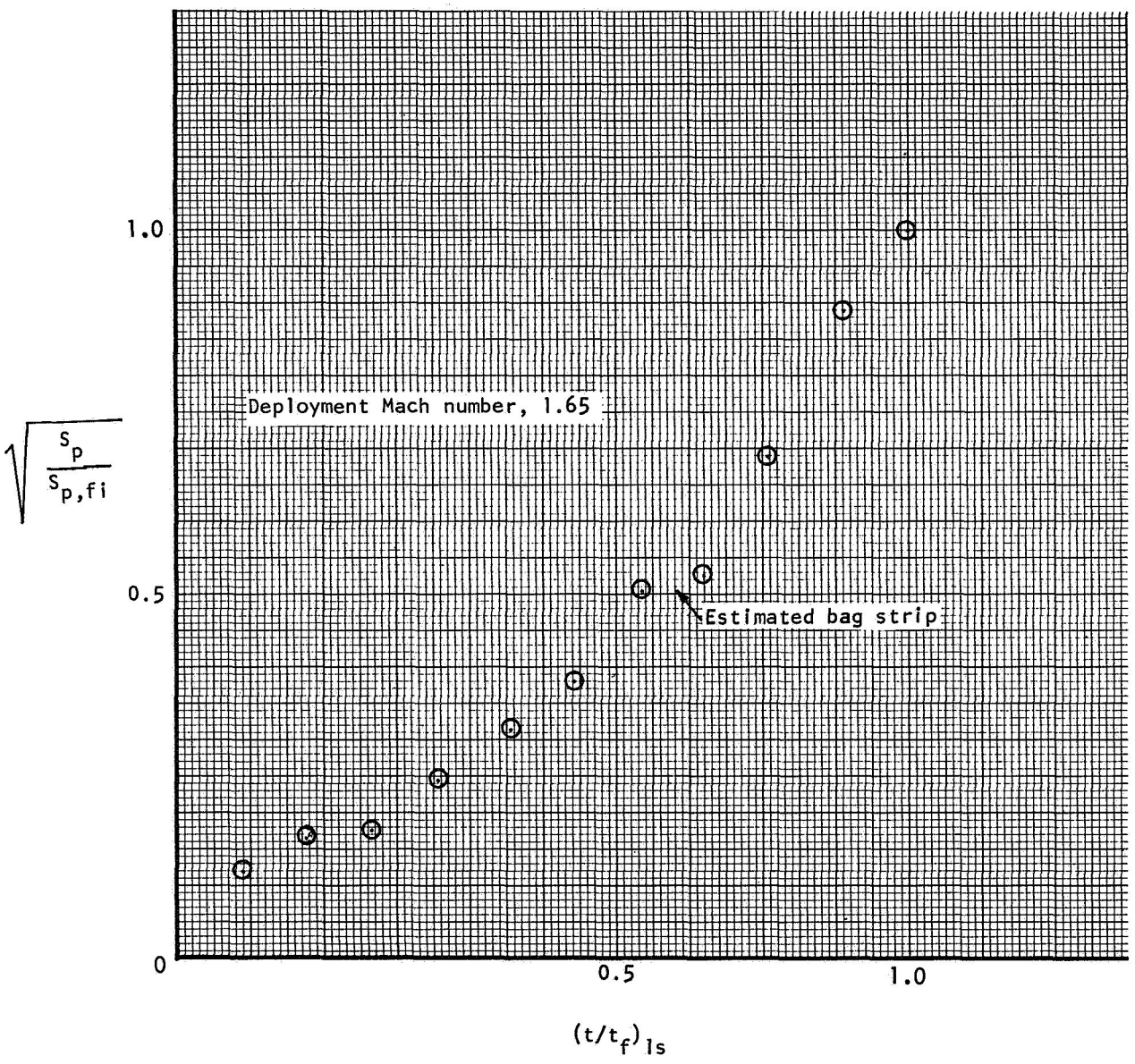

Figure 11.- Canopy growth parameter history for 54.4-foot (16.6-meter) cross parachute test.

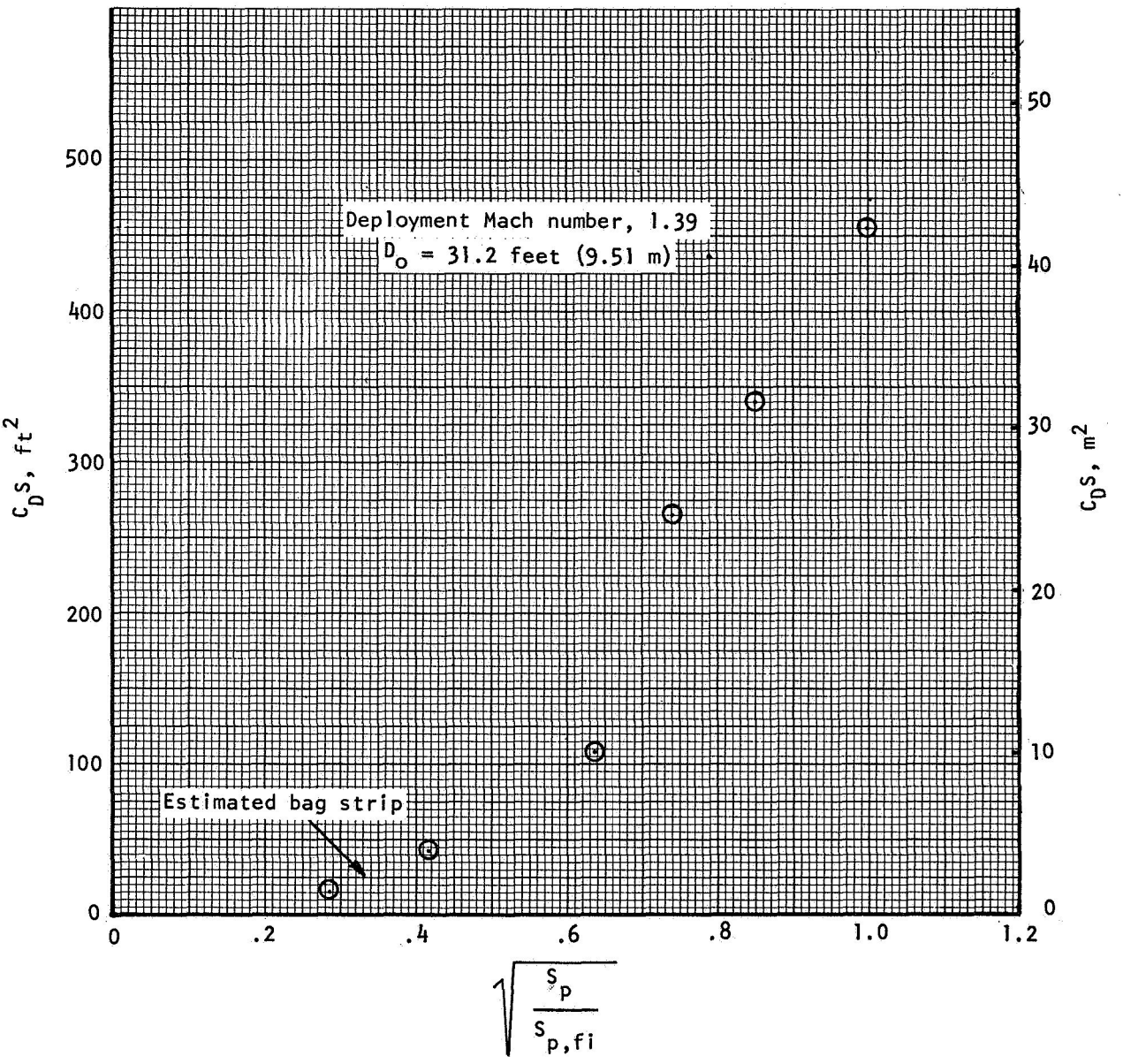

Figure 12.- Variation of drag area with canopy growth for modified-ringsail parachute.

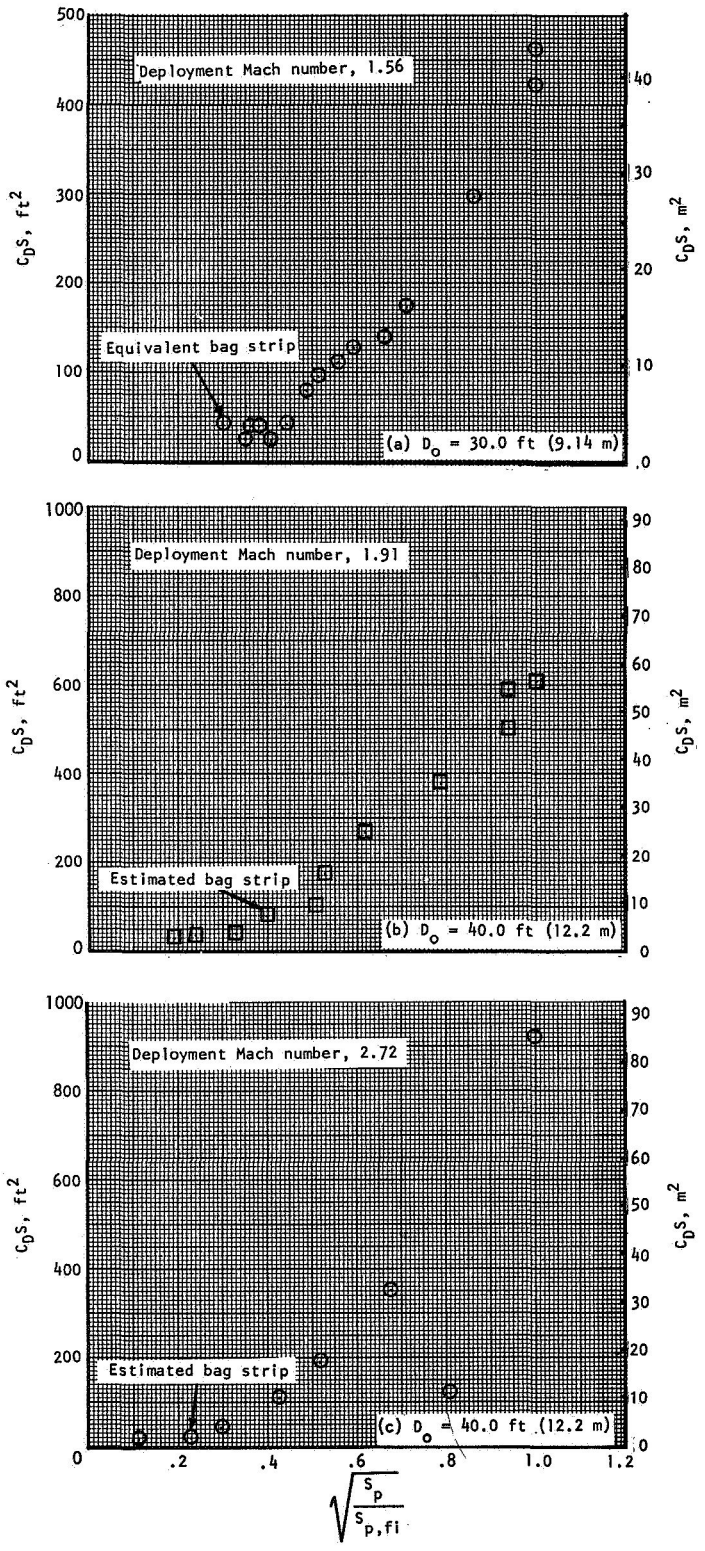

Figure 13.- Variation of drag area with canopy growth for disk-gap-band parachute.

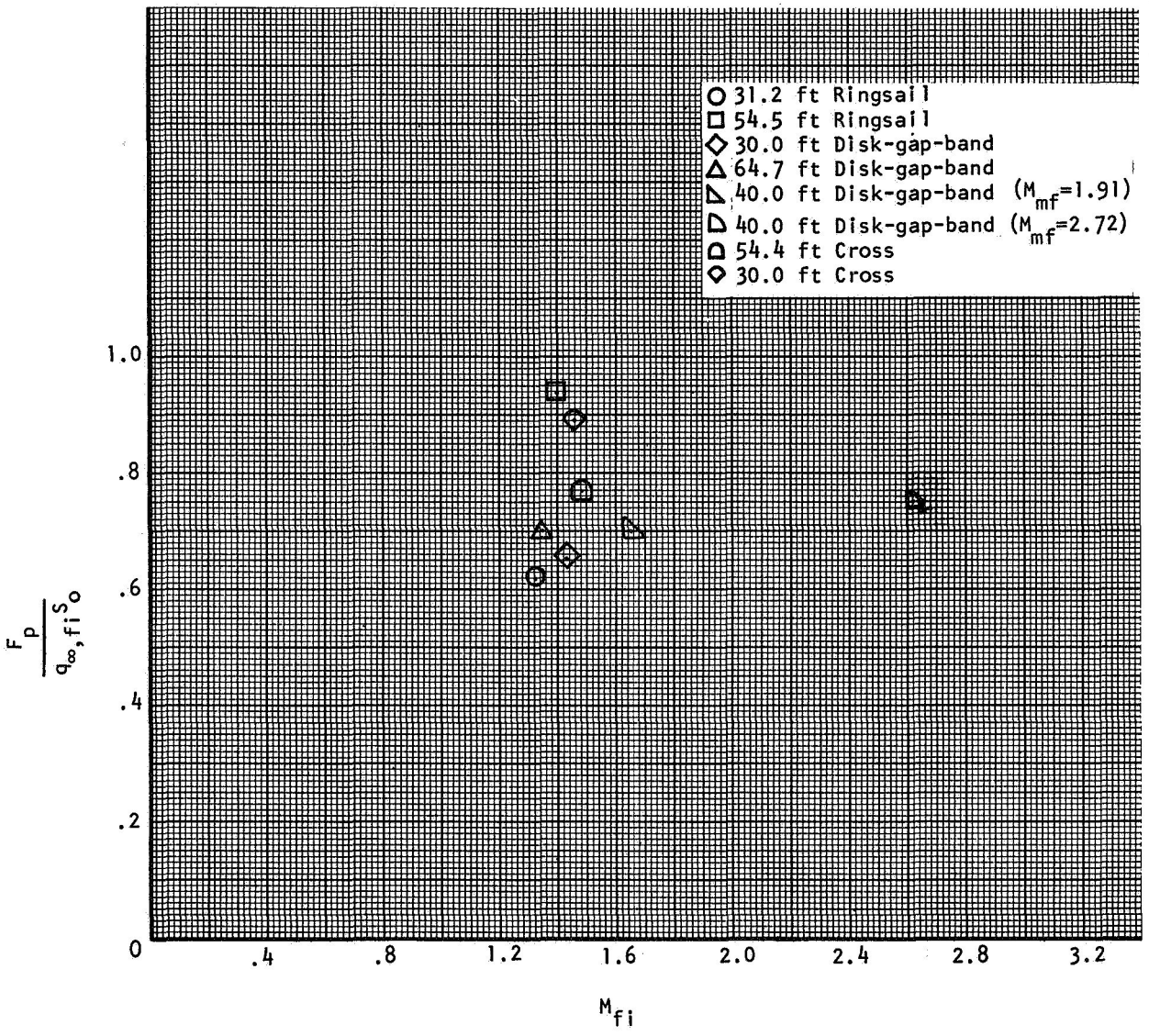

Figure 14.- Opening-force parameter as a function of Mach number. (1 foot = 0.3048 meter.)

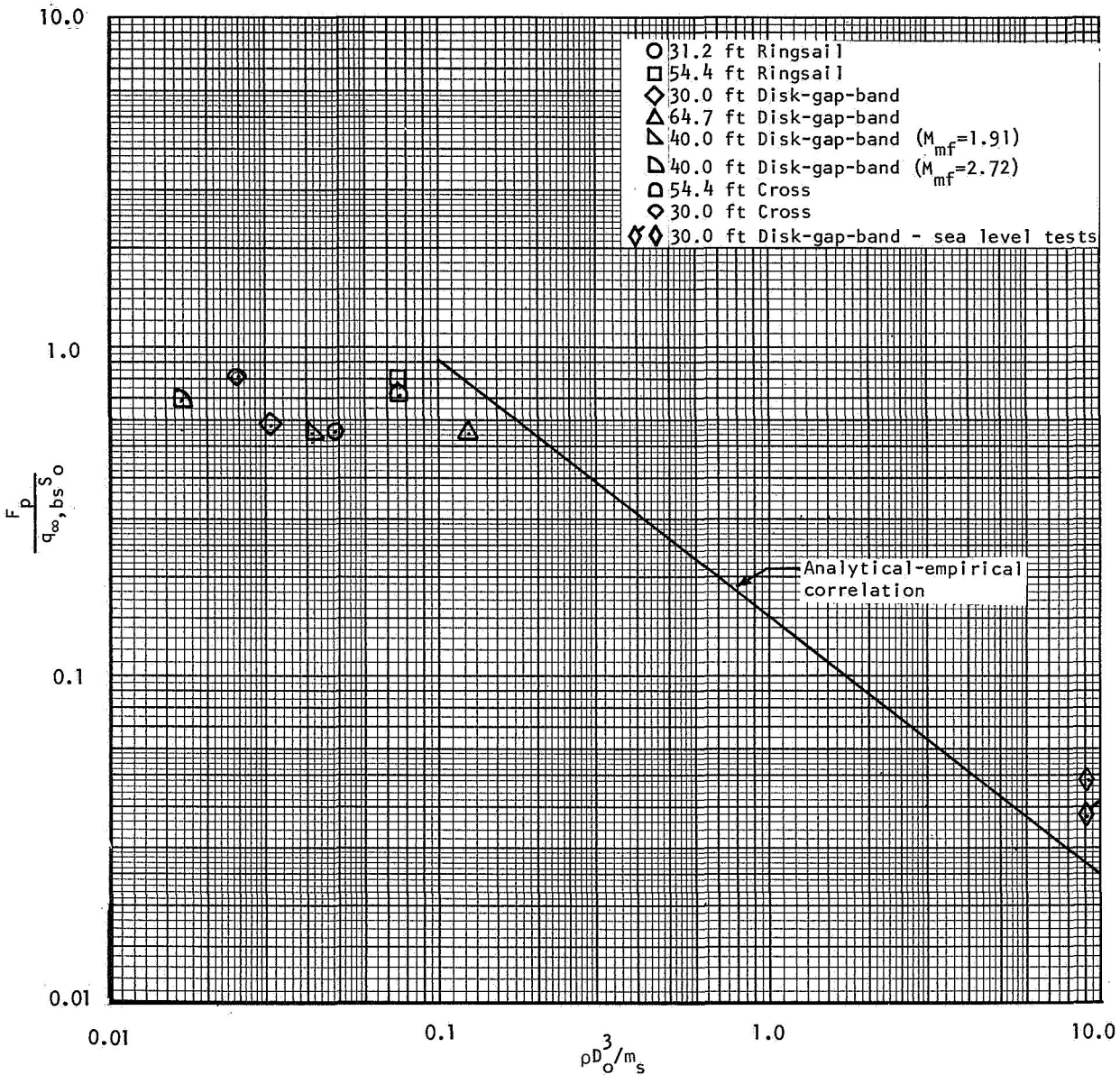

(a) Correlation based on bag-stripping conditions.

Figure 15.- Opening-force parameter as a function of mass ratio. (1 foot = 0.3048 meter.)

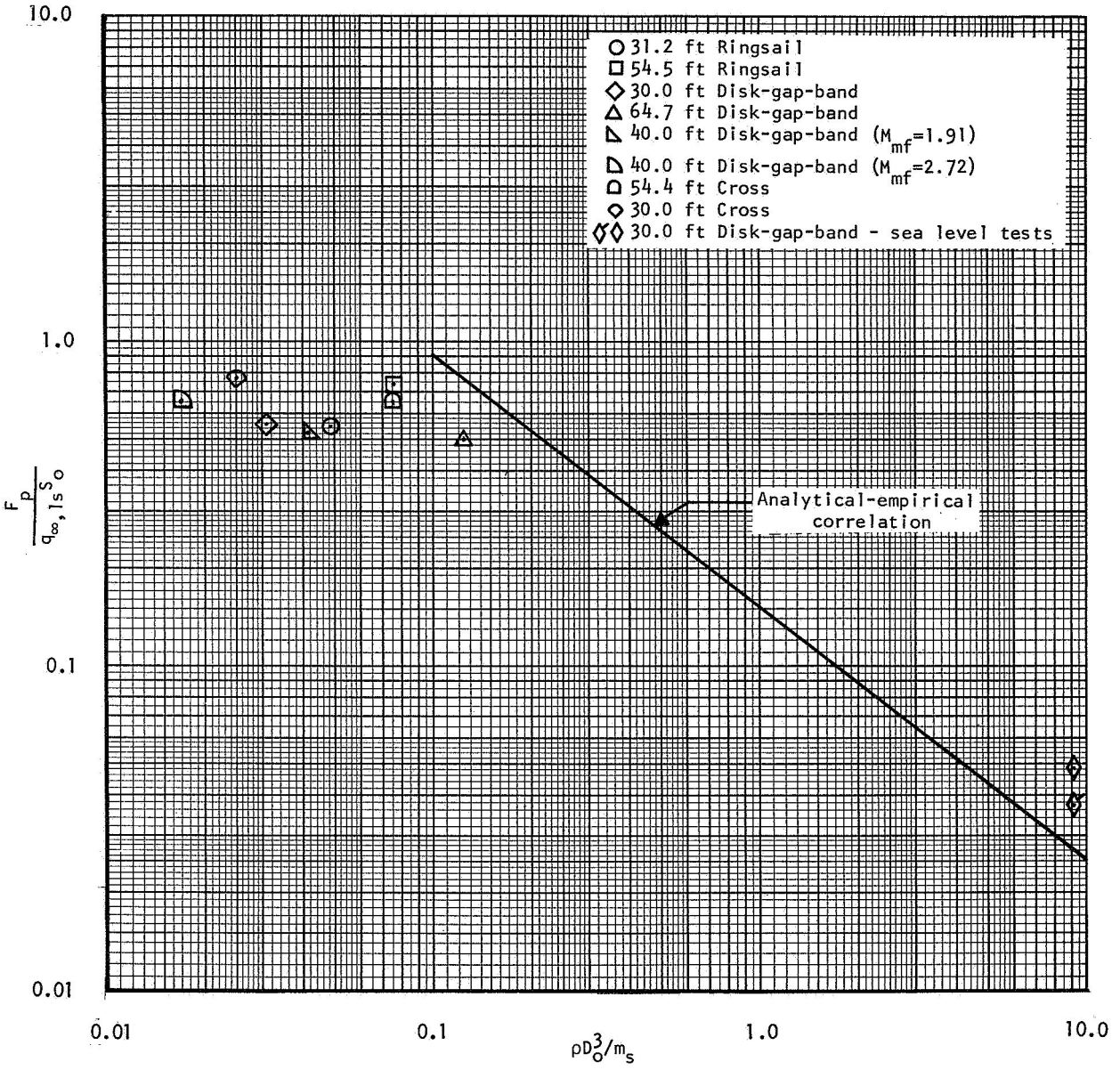

(b) Correlation based on line-stretch conditions.

Figure 15.- Concluded.

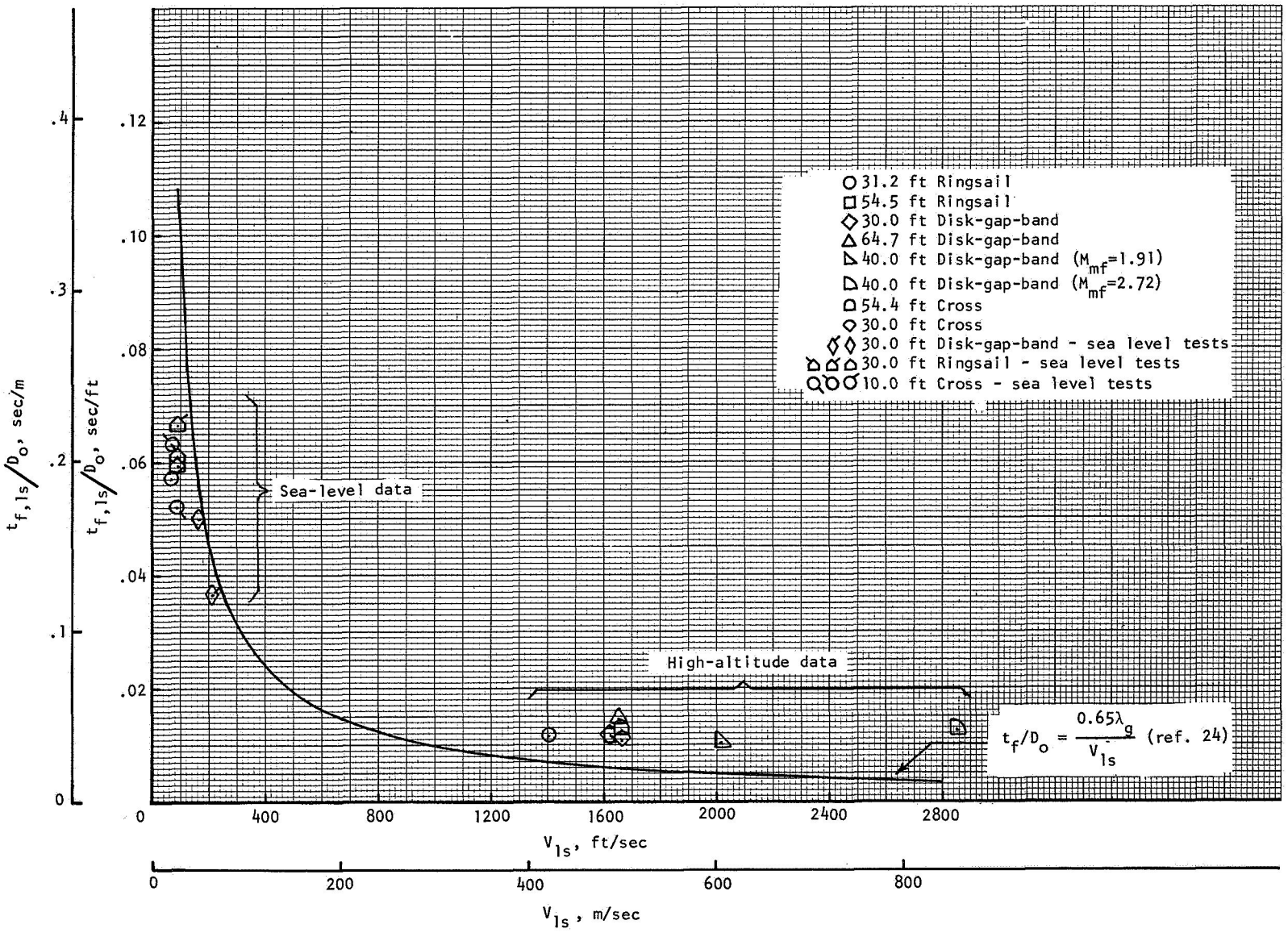

Figure 16.- Variation of filling-time parameter with velocity at line-stretch conditions. (1 foot = 0.3048 meter.)

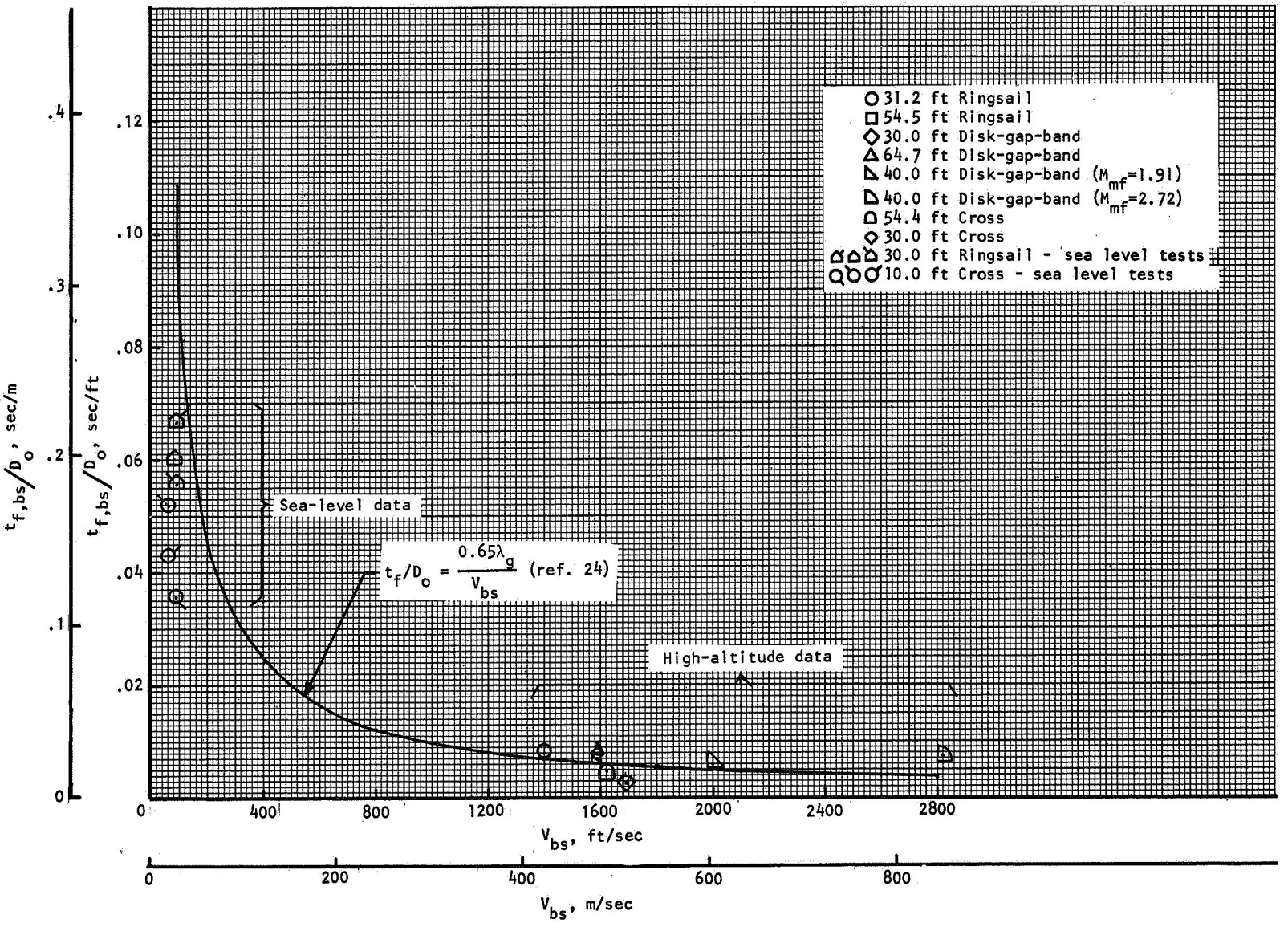

Figure 17.- Variation of filling-time parameter with velocity at bag-stripping conditions. (1 foot = 0.3048 meter.)

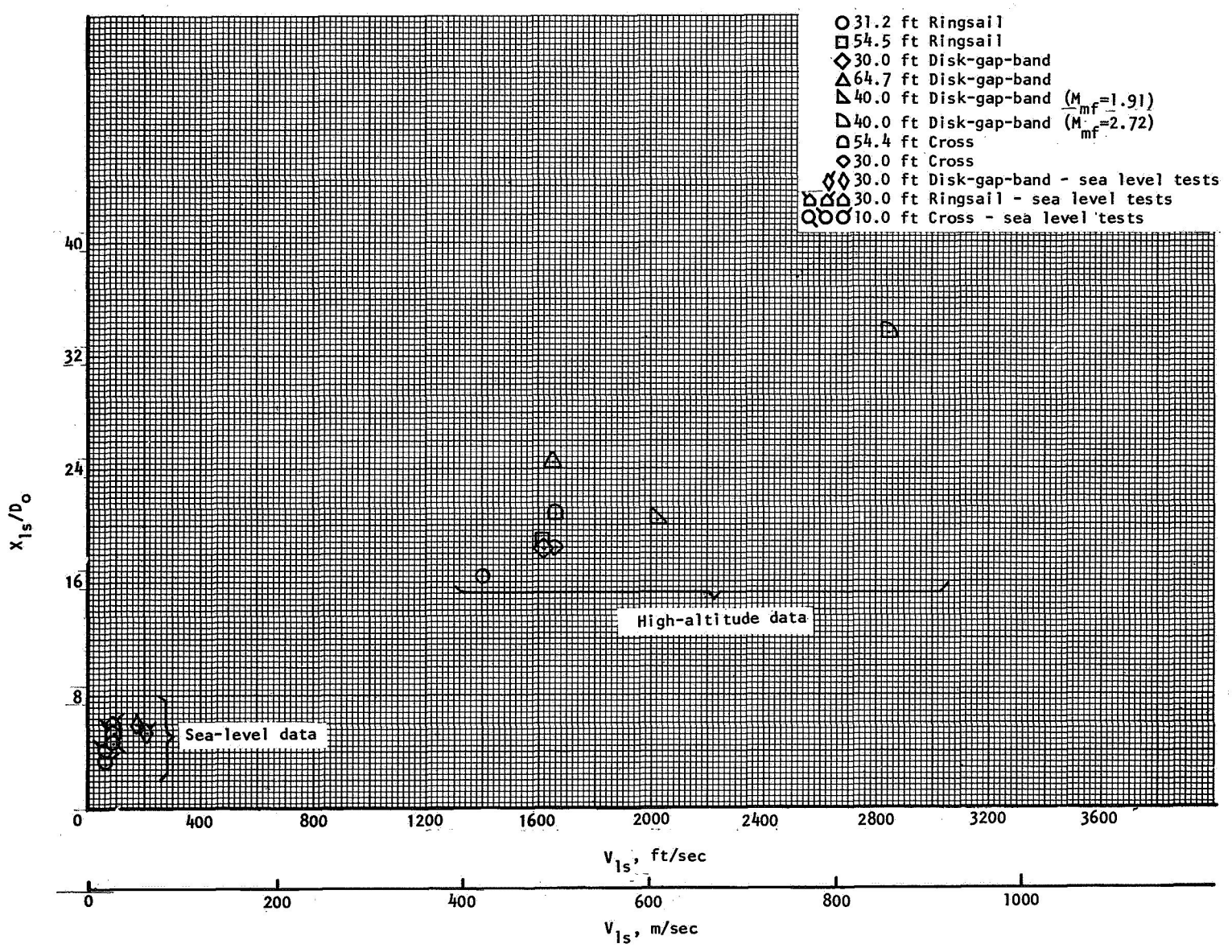

Figure 18.- Parachute inflation distance from line stretch. (1 foot = 0.3048 meter.)

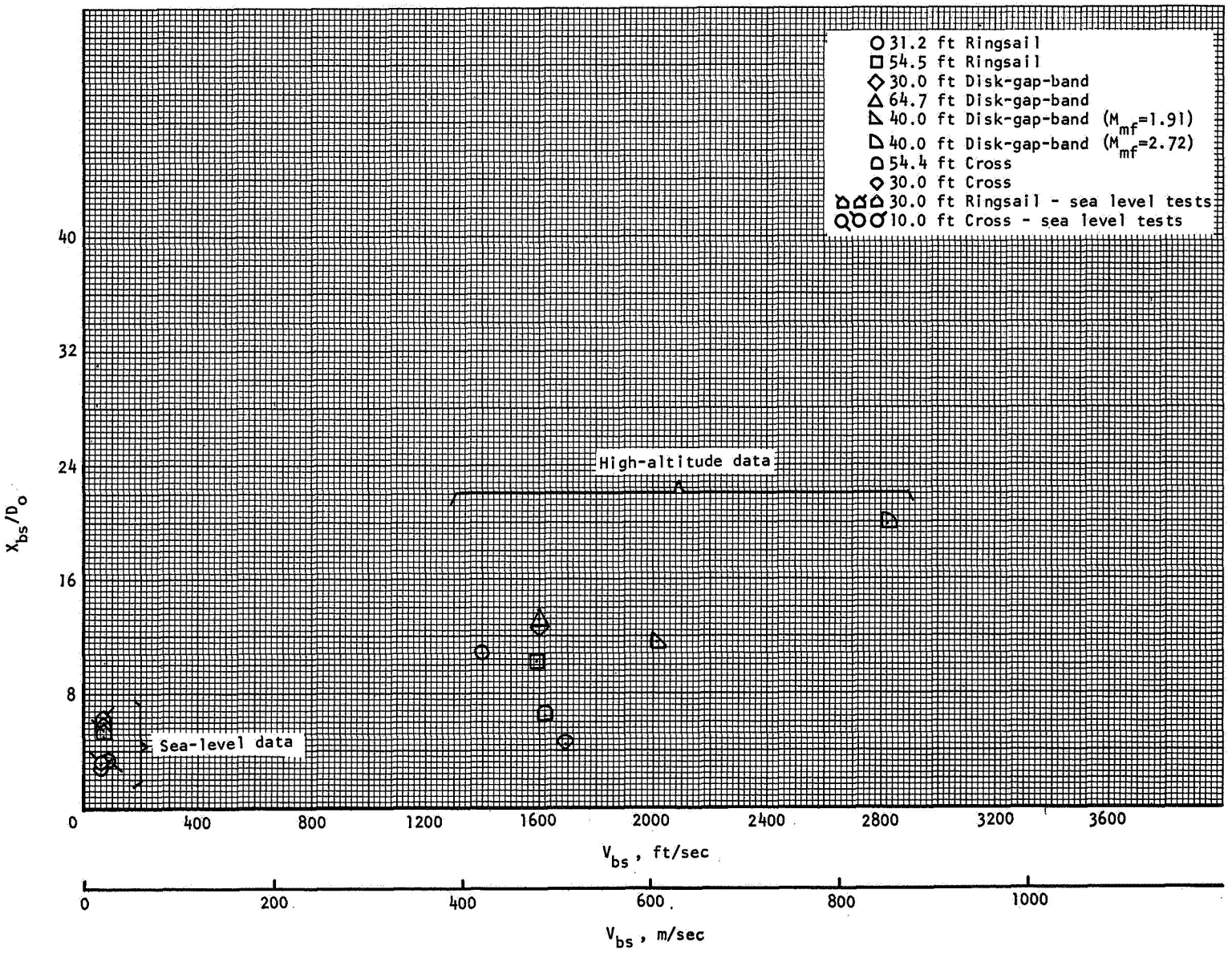

Figure 19.- Parachute inflation distance from bag strip. (1 foot = 0.3048 meter.)

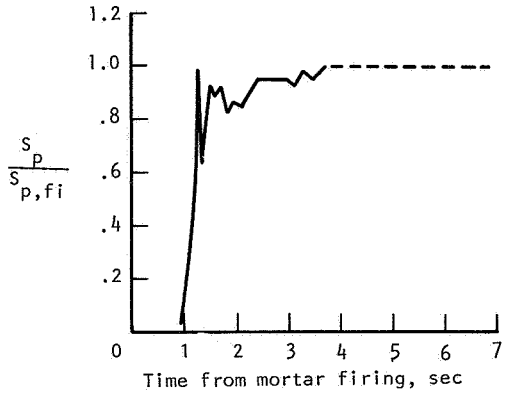

(a) 54.5-foot (16.6-meter) modified-ringsail parachute.

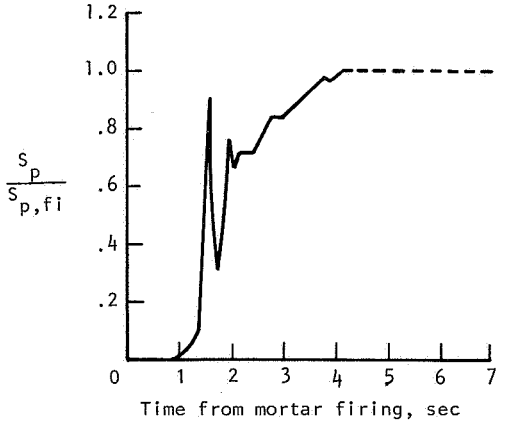

(b) 64.7-foot (19.7-meter) disk-gap-band parachute.

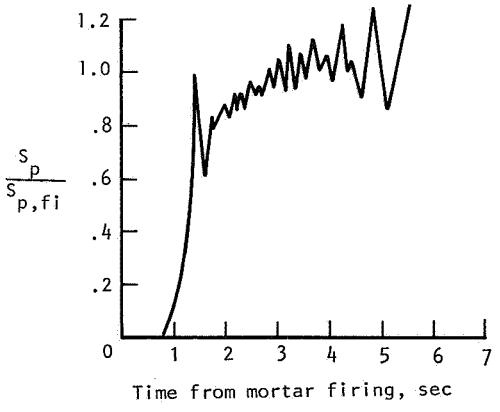

(c) 54.4-foot (16.6-meter) cross parachute.

Figure 20.- Projected-area time histories for deployments near Mach number 1.6.

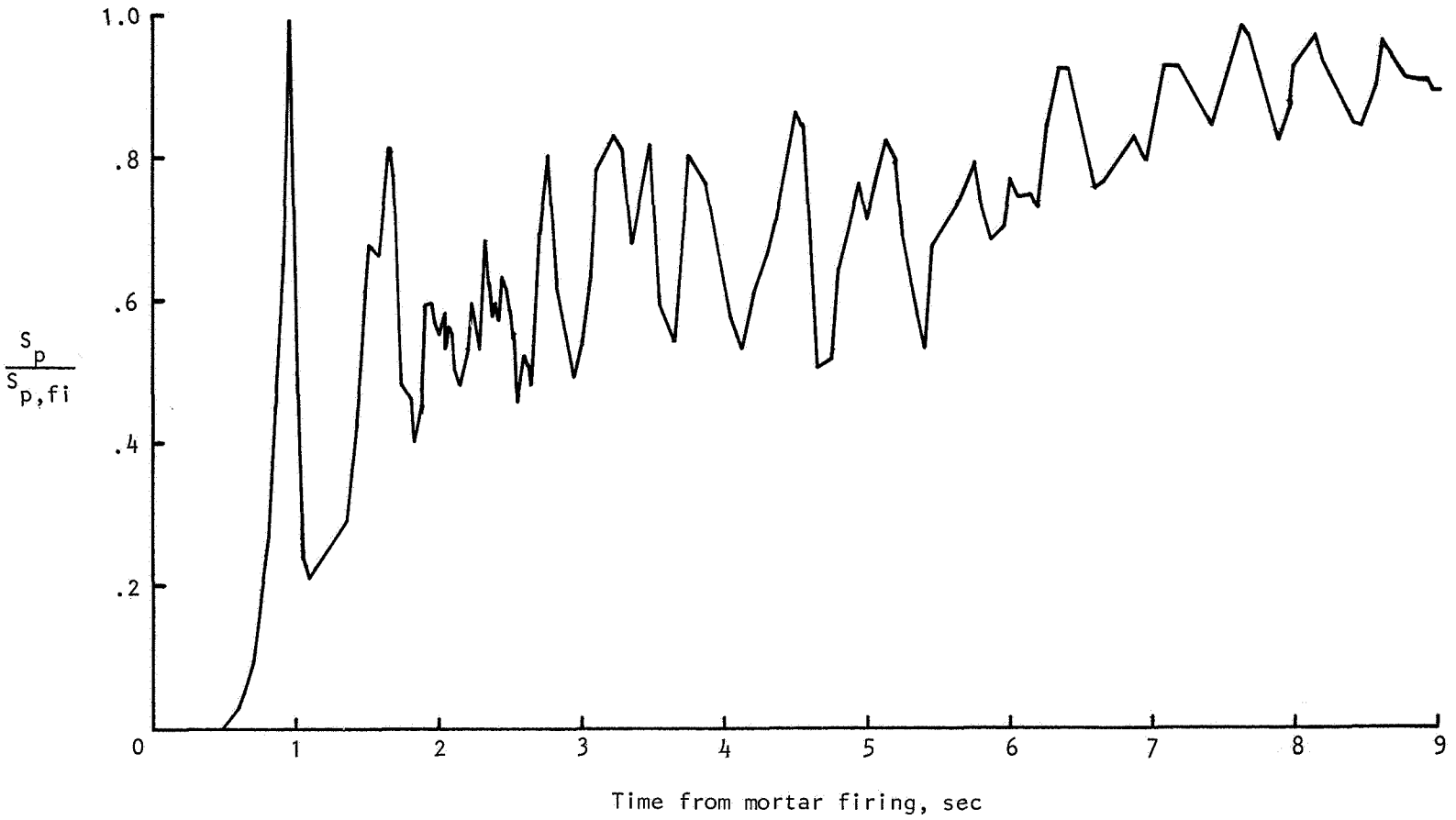

Figure 21.- Projected-area time history for disk-gap-band parachute deployed at a Mach number of 2.72.

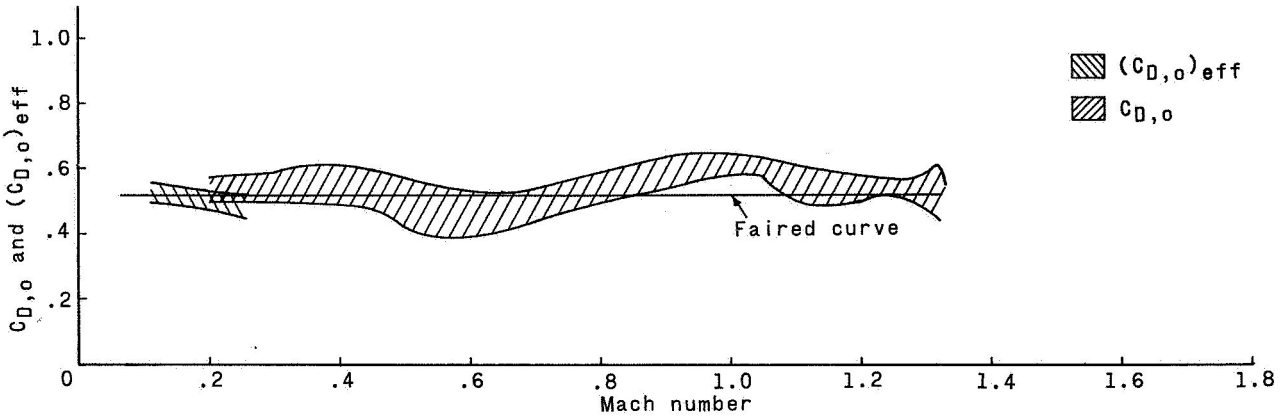

(a) D_0 = 31.2 feet (9.51 meters).

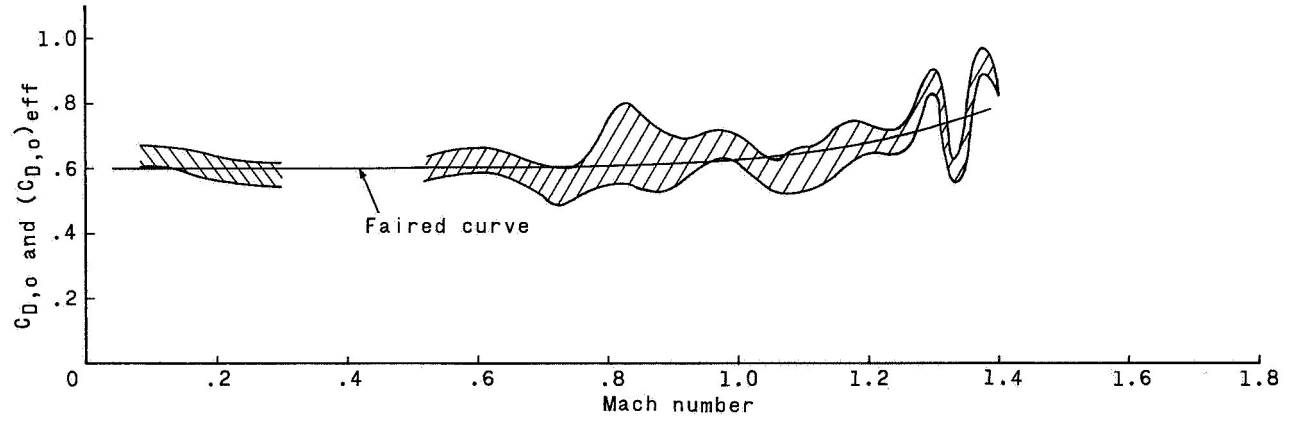

(b) D_0 = 54.5 feet (16.6 meters).

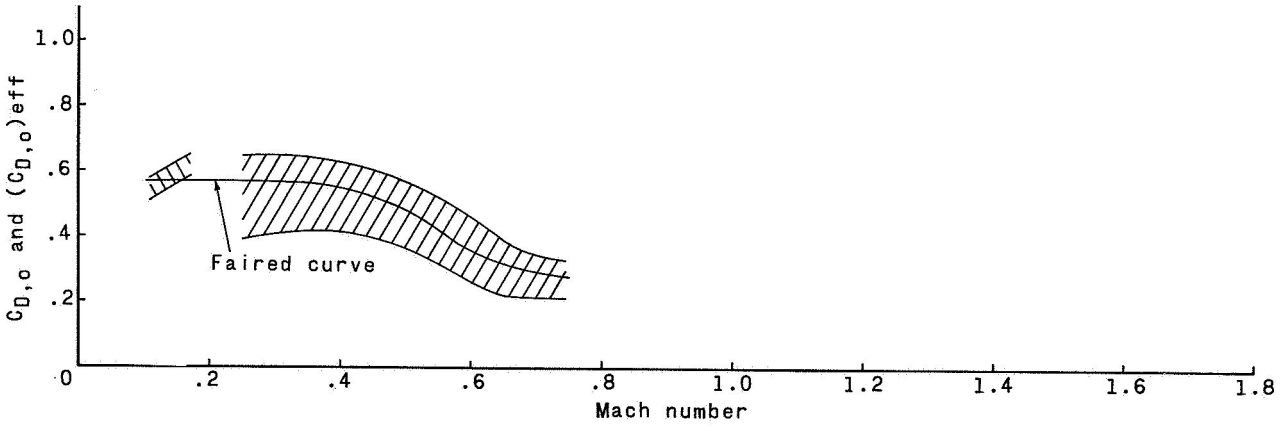

(c) D_0 = 85.3 feet (26.0 meters).

Figure 22.- Drag characteristics for modified-ringsail parachutes.

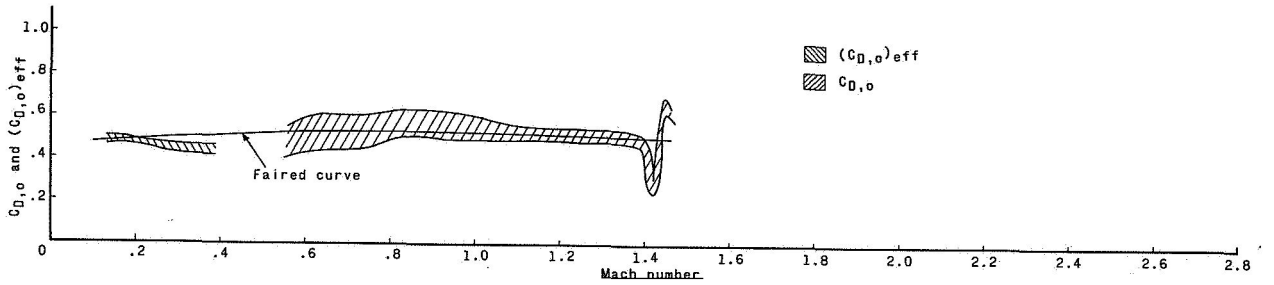

(a) D_0 = 30.0 feet (9.14 meters).

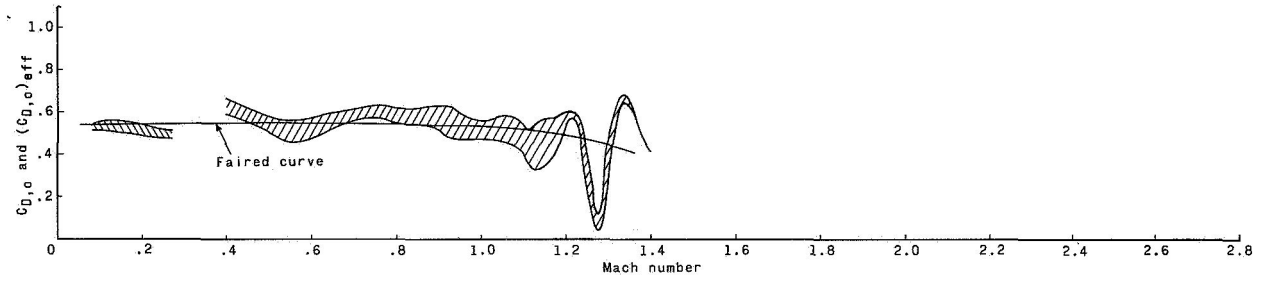

(b) D_0 = 64.7 feet (19.7 meters).

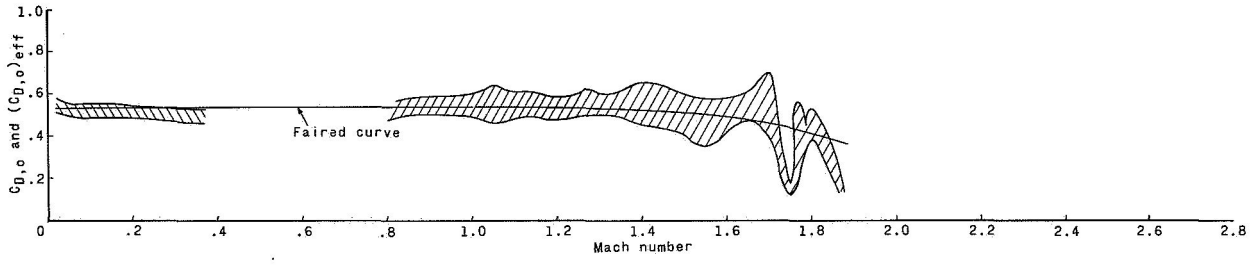

(c) D_0 = 40.0 feet (12.2 meters).

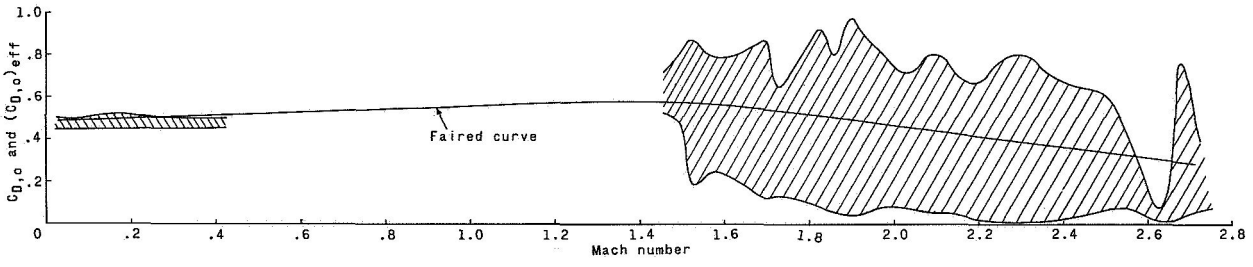

(d) D_0 = 40.0 feet (12.2 meters).

Figure 23.- Drag characteristics for disk-gap-band parachutes.

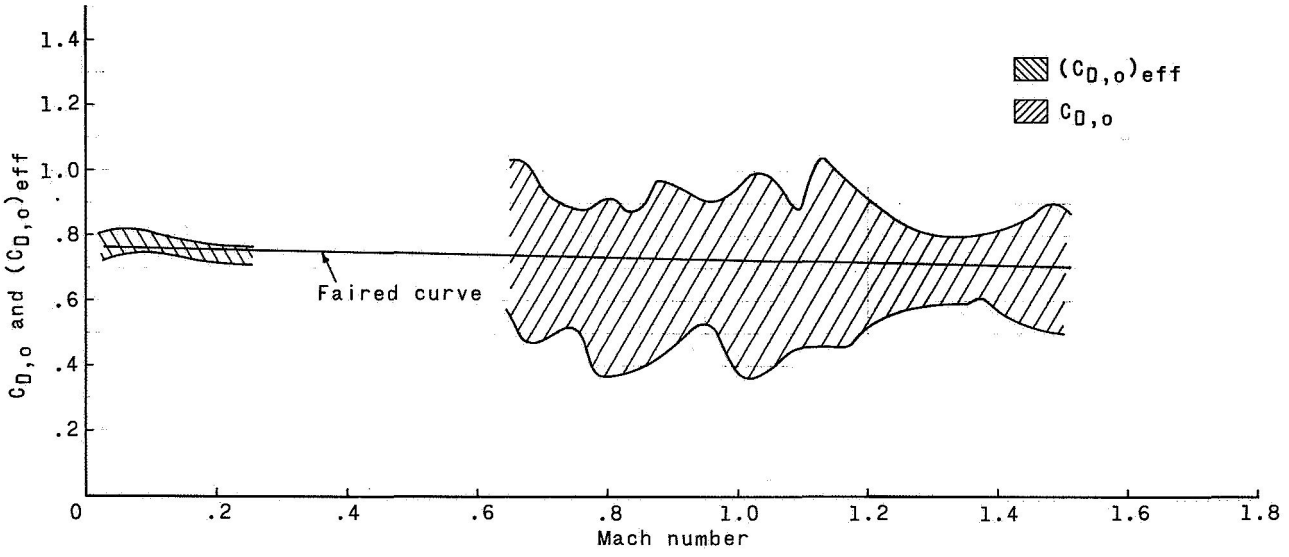

(a) D_0 = 30.0 feet (9.14 meters).

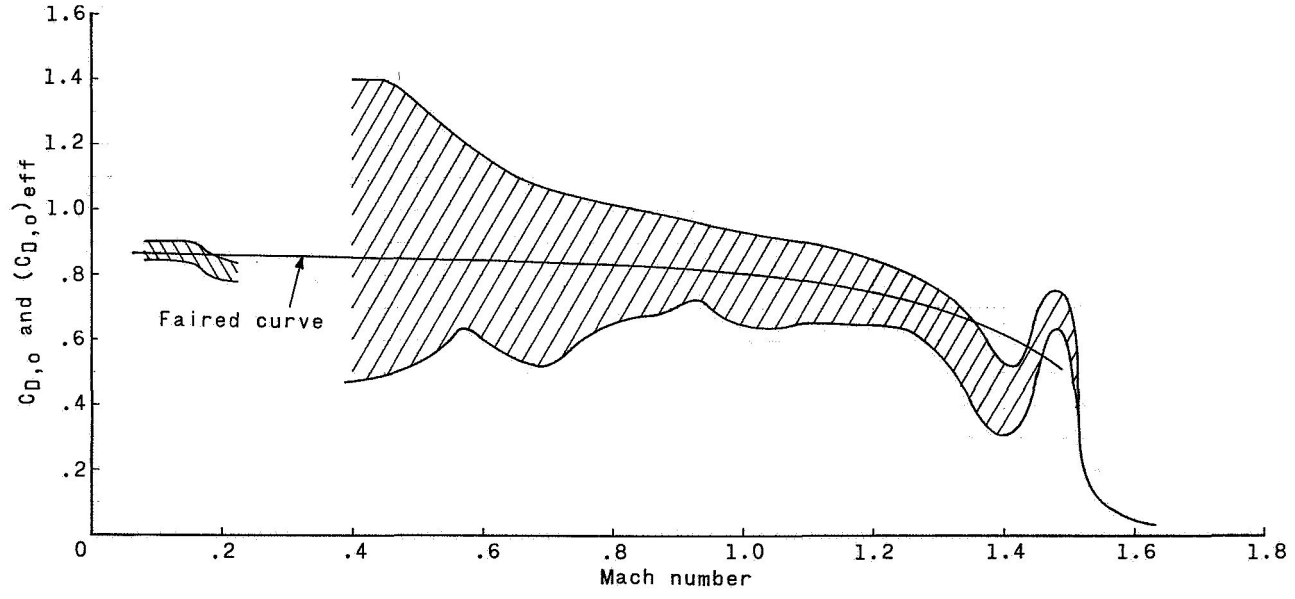

(b) D_0 = 54.4 feet (16.6 meters).

Figure 24.- Drag characteristics for cross parachutes.

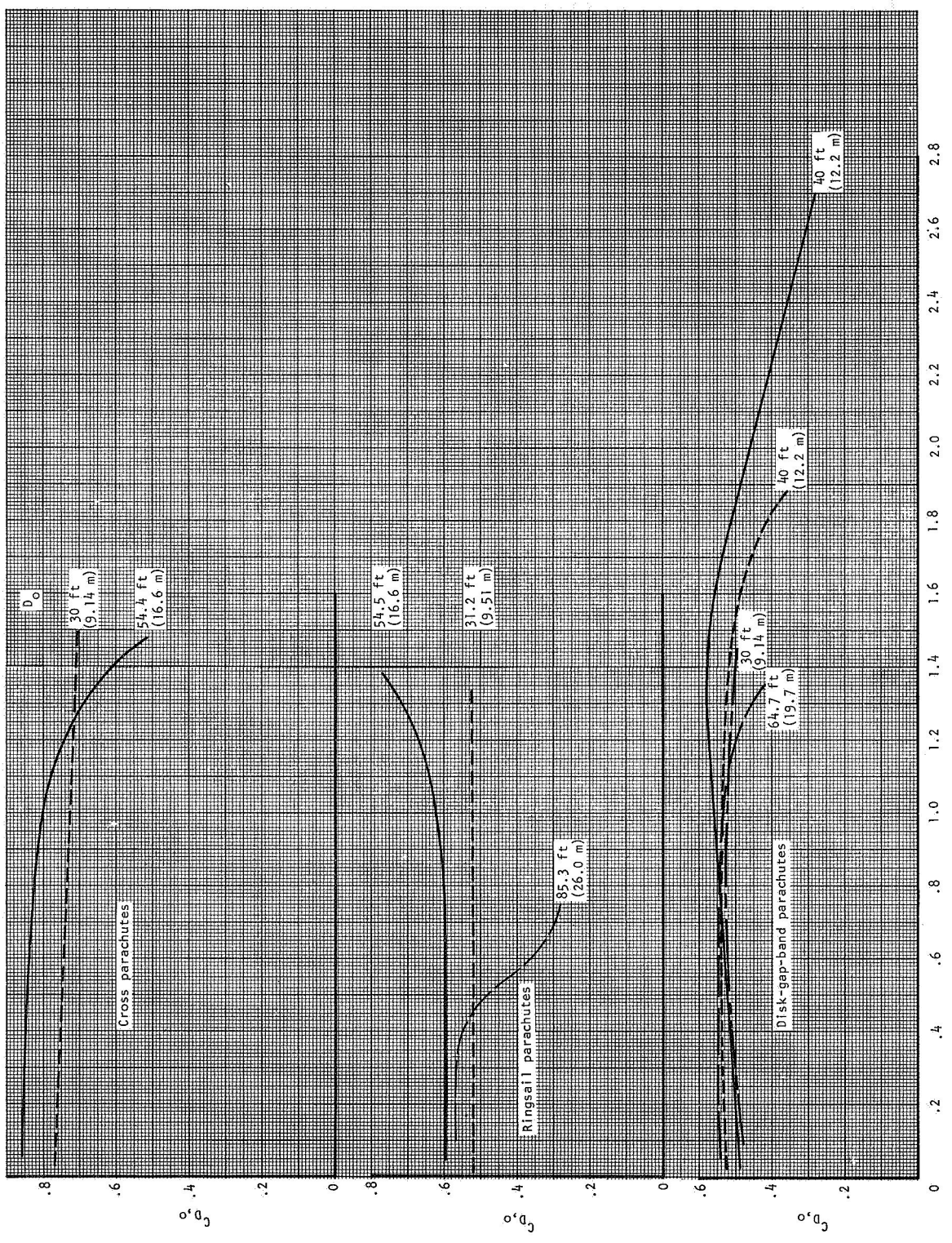

Figure 25.- Summary of faired drag histories.

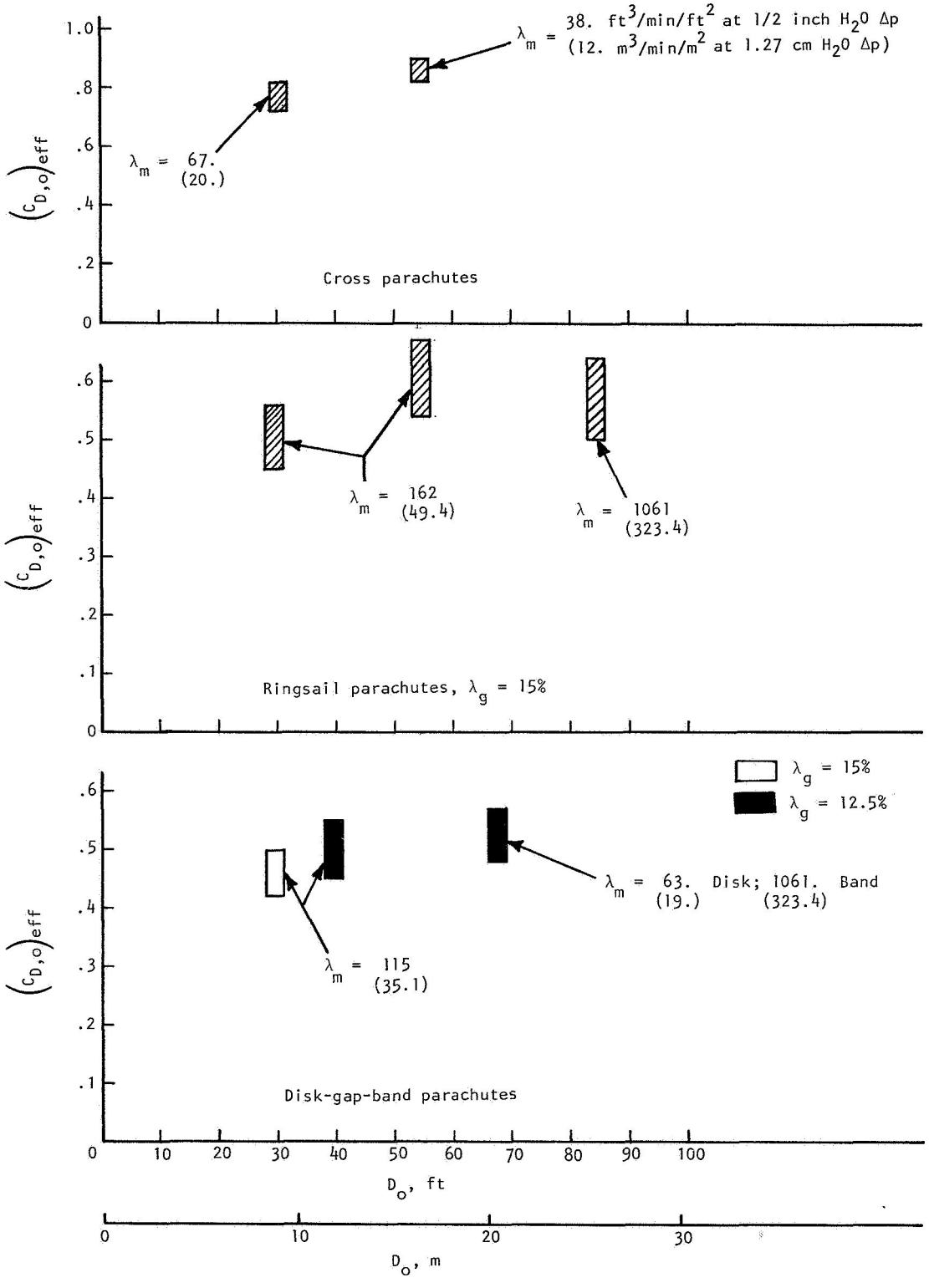

Figure 26.- Effective drag coefficient as a function of nominal diameter.

NASA-Langley, 1969 — 1 L-6361

"The aeronautical and space activities of the United States shall be conducted so as to contribute . . . to the expansion of human knowledge of phenomena in the atmosphere and space. The Administration shall provide for the widest practicable and appropriate dissemination of information concerning its activities and the results thereof."

—NATIONAL AERONAUTICS AND SPACE ACT OF 1958

NASA SCIENTIFIC AND TECHNICAL PUBLICATIONS

TECHNICAL REPORTS: Scientific and technical information considered important, complete, and a lasting contribution to existing knowledge.

TECHNICAL NOTES: Information less broad in scope but nevertheless of importance as a contribution to existing knowledge.

TECHNICAL MEMORANDUMS: Information receiving limited distribution because of preliminary data, security classification, or other reasons.

CONTRACTOR REPORTS: Scientific and technical information generated under a NASA contract or grant and considered an important contribution to existing knowledge.

TECHNICAL TRANSLATIONS: Information published in a foreign language considered to merit NASA distribution in English.

SPECIAL PUBLICATIONS: Information derived from or of value to NASA activities. Publications include conference proceedings, monographs, data compilations, handbooks, sourcebooks, and special bibliographies.

TECHNOLOGY UTILIZATION PUBLICATIONS: Information on technology used by NASA that may be of particular interest in commercial and other non-aerospace applications. Publications include Tech Briefs, Technology Utilization Reports and Notes, and Technology Surveys.

Details on the availability of these publications may be obtained from:

SCIENTIFIC AND TECHNICAL INFORMATION DIVISION

NATIONAL AERONAUTICS AND SPACE ADMINISTRATION

Washington, D.C. 20546